Alma Mater Studiorum – Università di Bologna

DOTTORATO DI RICERCA IN

Scienze Biotecnologiche e Farmaceutiche

Ciclo XXXI

Settore Concorsuale: 03/D1

Settore Scientifico Disciplinare: CHIM/08

Characterizing the functional dynamics of the Leak Potassium channel h-TRAAK through Molecular Dynamics Simulations under physiological conditions

Presentata da: Riccardo Ocello

Coordinatore Dottorato
Prof. Santi Mario Spampinato

Supervisore
Prof Maurizio Recanatini

Co-Supervisore
Dr. Matteo Masetti

Esame finale anno 2019

Let me take you down, 'cause I'm going to Strawberry fields.

Nothing is real and nothing to get hung about.

Strawberry fields forever.

Living is easy with eyes closed,

misunderstanding all you see.

It's getting hard to be someone but it all works out,

it doesn't matter much to me.

("Strawberry fields forever", *The Beatles* - 1967)

Abstract

Two Pore domain K^+ channels (K2P) are a specific family of channels whose functionality is finely tuned by a rich ensemble of chemical and physical stimuli. The ionic currents produced by these proteins are usually referred as ''leak'' or ''background'' potassium currents because they stabilize the resting potential of membranes to highly negative values close to the K^+ equilibrium potential. In particular, the human TRAAK channel (Twik Related Arachidonic Acid K^+ channel) is influenced by chemicals (anesthetics or drugs), and physical agents (pH, temperature, membrane stretching or bending).

Although the firsts experimental findings date back to early '00 a full comprehension of the gating mechanism and ion transport is still missing. Among the most influential theories on gating, we mention the two states hypothesis suggested by MacKinnon thanks to the crystal structure availability. The existence of an atomistic model paved the way to furthers investigations, as well by using theoretical approaches.

In this context, exploiting in silico techniques belonging to computational biophysics, we provided a comprehensive characterization of the channel behaviour. Advanced simulating conditions were used, with the purpose of mimicking as close as possible the real protein behaviour, and some of those key-biases playing a modulation role of channel activity.

By using Molecular Dynamics simulations, several protocols were applied to simulate hTRAAK in presence of different conditions: i) membrane stretching, ii) ions concentration gradients, iii) applied electrostatic potential. These strategies were chosen to gain new insights into the putative conductive state of the channel, promoting the translocation of K^+ ions through it.

Table of Contents

List of Figures

1 Introduction

1.0 Ion Channels

The nervous signalling is one of the most common and complex processes shared by eukaryotic cells in nature. Its main function is to put in communication different regions of the body, sending signals from one district to another. This kind of process is mediated by electrochemical waves traveling along fibers called axons or by chemicals released onto other cells.

The main proteins involved in the former process are ions channels, specialised and often selective pores embedded into biological membrane cells, which are implicated in the active or passive charges transport from cytoplasmic to extracellular side and vice versa. The peripheral nervous system (PNS) consists of motor and sensory neurons, whose clusters are called ganglia, and nerves connecting them to each other and to the central nervous system (CNS). Sensory neurons are activated by inputs impinging on them from outside or inside the body. They send signals that inform the central nervous system of ongoing events. Together with transporters, ion channels are entities able to accomplish electrical charge transfer through the cell membrane. Every event in which a signal transduction takes place is related to ion channels; they bear the same relation to electrical signalling in nerve, muscles, and synapse, as enzymes bear to metabolism. It can be said that as the enzymes catalyse organic reactions, ion channels catalyse permeations process otherwise impossible to achieve.[1] Even though their diversity is certainly less broad than that of enzymes, there are still many types of ion channels which differ each other for ion species translocated (Na^+, K^+, Ca^{2+}, Cl^-), selectivity, shape, and distribution across human body.

Potassium channels play a key role in a plethora of physiological processes essential for life: i) rapid and selective translocation up to the diffusion rate of K^+ down to the electrochemical gradient across cellular membranes; ii) resting potential in excitable cells restoration; iii) regulation of hormone and insulin secretion; iv) regulation of the action

potential in cardiac muscle and maintainement of vascular tone.[2–4] Obviously, all of these functions, as well as the associated regulations mechanism are strongly dependent on the tissues distribution.

1.1 K^+ Channels

The primary catalytic role of potassium channels is the K^+ ions shuttling across cell membrane. This specific function is carried out in bacterial and eukaryotic cells, thanks to a highly conserved structural motif called Selectivity Filter (SF).[5] The main task of SF is to allow potassium translocation from one side to the other of a membrane double leaflet, at rates comparable to the diffusion limit. The SF is formed by a very easy to recognise primary sequence, whose shape and sequence are shared among all classes of channels.[5]

Nowadays K^+ channels are grouped in four mains classes (Figure 1), which differentiate each other through the primary gating mechanism, i.e. by the principal agent able to modulate the transition between open and closed states.[6] In the first class, the **voltage gated** channels (i.e. K_V channels, Shaker), the pore opening is dependent upon the movement of a charged voltage sensor. All channels belonging to this class are involved in the depolarisation phase of the action potential in excitable cells (neurons, cardiac cells).[7] The second class is formed by **ligand gated** channels, where the conductive conformation is promoted by ions, small molecules or proteins able to bind the channel in specific regions (BK_{Ca} sub-class where the ligand is Ca^{2+} ion).[8] As third class the **inward rectifier** K^+ channels (K_{IR}) are those involved in reuptake activity, in which potassium ions are moved by the extracellular environment to the cytosol during the repolarisation phase of action potential; K_{IR} activity is ligand regulated.[9] **Leak** or **background** potassium channel (K2P) represent the last class, which comprise all those proteins involved in the maintaining of resting potential of excitable cells. The function of leak channels is influenced by a wide range of physical and chemical agents (like anaesthetics, temperature, pH variation, membrane pressure, polyunsaturated fatty acids).[10]

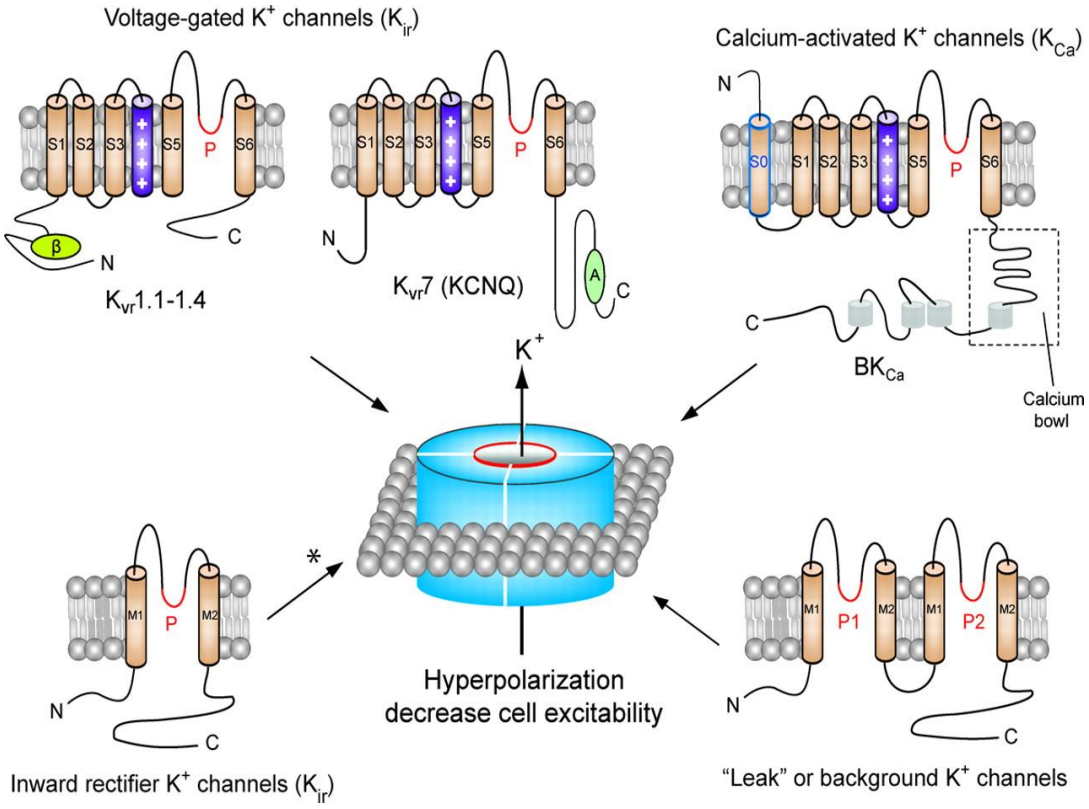

Figure 1. Four classes of Potassium channels.

Thanks to advances in X-ray crystallography, in the last two decades several ion channel structures have been identified, giving a fundamental contribution to the investigations in biochemistry, and in general in structural biology.[11] This is mainly due to the efforts of Nobel laureate Prof. R. MacKinnon, who published almost twenty years ago the first K^+ channel crystal structure.[12] The KcsA channel protein has been for several years, and still is, the prototype of K^+ channel used to investigate all relevant properties of this family, providing crucial mechanistic and structural insight on the molecular basis of K^+ selectivity and conduction. In general, K^+ channels, are assembled as multimeric proteins (homo or hetero tetrameric K_V, BK, K_{IR}, homo dimeric K_{2P}). The core of the tetramerization is the pore domains where each monomer contributes to the formation of the characteristic motif of the SF. The prototypical architecture of a K^+ channel monomer is constituted by two transmembrane α-helices (TM) and a small loop in between (called P LOOP), as is show in Figure 2, where a KcsA monomer is highlighted (referred to as 2TM/P). The tetramerization of a single monomer is a typical structural feature of for the K_{IR} channels.

Although each class has its distinctive features, this canonical architecture (formed by 2TM/P domains) is an universal element; for example, in the K_V channels (Figure 1a, 6TM/P) four α-helices (from S1 to S4) precede the 2TM/P domain. Other variations are found in 8TM/2P or 4TM/2P channels where two pore-forming domains (2TM/P) are present for each monomer. Quaternary structures of these families (K2P channels) are also different considering their dimeric assembly. Thanks to the tetrameric or pseudo tetrameric (literally dimeric) shape adopted, in any case four P LOOP originate the ion permeation pathway in the protein core, which is orthogonally located to the cytoplasmic membrane.

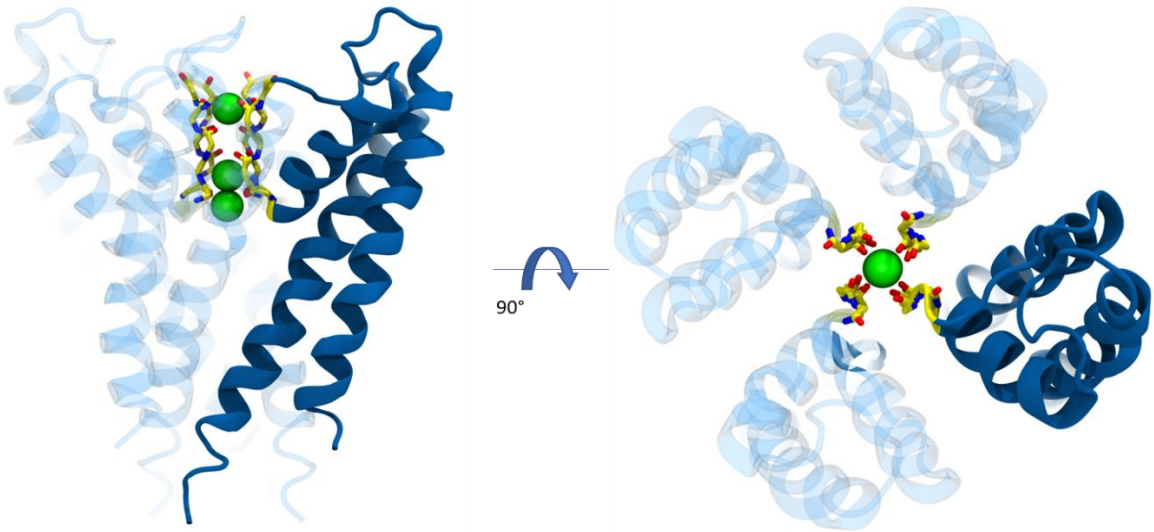

Figure 2. Side and top view of KcsA channel. Highlighted in dark blue is a single monomer with (2T/P). In yellow represented in tubes, the core domain Selectivity Filter (SF).

1.2 Background currents: physiological role of K2P

Although the leak (or background) currents, were already identified in the middle of the last century, the responsible biological entities were still unknown until 1995. Before the discovery by Ketchum and Goldstein of the first two pore domain outward rectifying K^+ (TOK1) channel proteins from *Saccharomyces cervisiae*,[13] the existence of background currents across cellular membrane have been predicted by the pioneering work of Hodgkin and Huxley.[14] These outward currents are involved in maintaining the resting potential and are essential for the potassium homeostasis of cells.

The human progenitor of K2P channels, firstly identified and expressed in humans cells, was the Tandem pore domain in a Weak Inward rectifying K^+ channel[15] which is able to show outward or inward currents upon depolarization or hyperpolarization, respectively. Between 1996 and 2003, the family of cloned mammalian background K^+ channel was enriched of 14 further members divided in 6 subfamilies: TWIK, TREK, TASK, TALK, THIK, TRESK. The typical protein architecture is the main feature shared by them, although the sequence similarity is not that high as expected (less than 30% of sequence similarity between TWIK-1 and TREK-1).[16]

The name of each sub-family is strictly related to the structural similarity to the parent channel (TWIK), to the main functions, and/or the chemical/physical agents responsible of their functional properties:

- TREK → Twik-Related K+ channels
- TASK → Twik-related Acid Sensitive K+ channels
- TALK → Twik-related Alkaline pH activated K+ channels
- THIK → Tandem-pore domain Halothane Inhibited K+ channels
- TRESK → Twik-related Spinal cord K+ channels

The grouping criteria accepted today are essentially based only on sequence homology. TASK-2 for example, was initially grouped in TASK family based on its sensitivity to extracellular pH even thought their low sequence similarity; it has been subsequently reassigned to TALK family. TWIK-related Arachidonic Acid K^+ channel (TRAAK), show 54% of sequence identity to TREK-1 channel (PNAS_Bichet_2016), thus belong to TREK family (Figure 3)

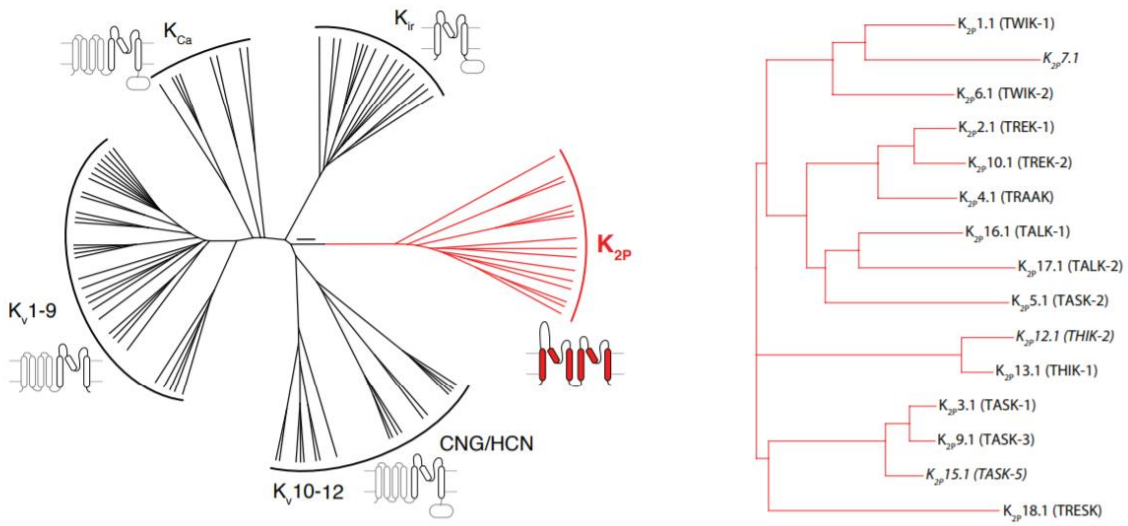

Figure 3. Phylogenetic tree of K^+; in red K2P channel family (adapted from ref.[17])

In contrast to the well-known Inward rectifying or Voltage gated K^+ channels, the conduction of K2P protein is not strongly voltage dependent, which means that the opening probability of the channel is the same at all membrane potential values and is also independent by K^+ concentrations on the two sides of a membrane. These are two of the features that characterize an "ideal background" K^+ channel, which should follow the Goldman-Hodgkin-Katz equation in [K^+] symmetrical condition. The behaviour in absence of voltage dependency makes them able to conduct currents in both directions, such that a rapid change of the membrane potential results in a prompt response in term of background current. Thus, a voltage step in a voltage-clamp experiment induces a square wave like K^+ current, which is in open contrast with the classical Kv or Kir channels behaviour (Figure 4). While voltage-gated channels show a delay before the current flow (depending on the progressive conformational changing upon depolarization thanks to the

voltage sensor that activates the channel), the same does not hold for K2P channels which are readily open to conduct currents.[18]

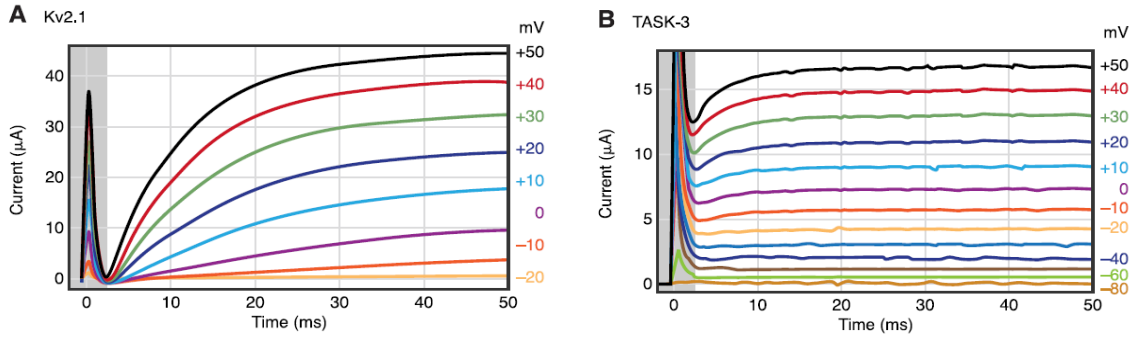

Figure 4. Current traces of Voltage gated (Kv1.2, A) and K2P (TASK-3, B) channels. The currents were elicited by voltage step from -80 to +50 mV in 10 mV increments in a solution of 2mM [K+]. After a transient of 2.5 ms, Kv1.2 is not active yet, whereas TASK-3 is close to its maximum, showing a rapid response to the membrane polarization. Moreover TASK-3 is stilll active at strongly negative potential (-80 mV), in contrast to voltage gated wich start to conduct since -20mV adapted from ref.[18]

Another characterizing aspect of "ideal background" channels, is that the outward rectification showed during their activity is independent by K^+ concentration gradients; they show Ohmic trends i.e. linear correlations between applied potential and induced currents (I-V curves, Figure 5), when [K^+] is equal on the two sides of plasma membranes. But when the [K^+] is high intracellularly and low extracellularly, only a larger outward current is observed even at negative potential (but "more positive" compared the resting sate).

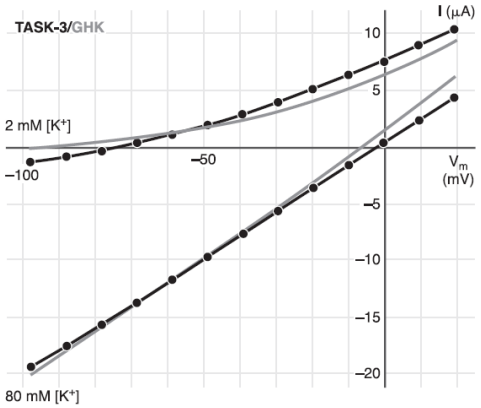

Figure 5. Current-Voltage relation in a depolarizing voltage step experiment from -100 to 20 mV. Linear (Ohmic) trend observed under quasi-symmetrical ([K+] 80mM in the extracellular) conditions. Outward rectifications under 2mM extracellular [K+] (adapted from ref. [18]).

Although K2P channels do not fully satisfy the above criteria (due to a weak or absent voltage dependency, rectification in symmetrical [K+], etc.), they provide the best approximation of leak currents compared to other K^+ channel classes.[18]

The expression of K2P channels throughout the human body and the high distribution in CNS has recently turned interest on them as potential drug targets.[19,20] It is now well accepted that they are involved in the regulation/stabilization of membrane potential below the firing threshold of excitable cells, thus they are directly involved in the transmission of electrical impulses. Moreover, they are responsible for restoring basal currents and, strongly connected to this, they are also able to influence duration, frequency and amplitude of action potential. Increased leak currents stabilize cells at hyperpolarized voltages, whereas leak suppression allows depolarization and excitation. A plethora of chemical agents or physical stimuli regulate their activity, including pH, lipids, neurotransmitters, G-protein coupled receptors and mechanical stretch. The regulation mainly take place (as for other ion channels) modulating the opening probability and unitary current. Considering the crucial emerging roles in cell signalling, K2P channels have been identified as important targets of several widely employed drugs, including anaesthetics, neuroprotectants and antidepressants.[21]

1.3 The TREK channel family: activity and modulation

TREK-1, TREK-2 and TRAAK are the members of the most studied family of K2P channels, which exhibit a polymodular behaviour. TREK genes expression is widespread in mouse, rat and human, and many splices variants were reported to exhibit tissue-specific expression. Mouse TREK-1 for example is abundant in brain, lung, kidney, heart and gastrointestinal GI-tract in two variants of different length, while human expression is limited to brain and (GI)-tract.[21] High levels of expression are also present in hippocampal glutamate-containing neurons as well as in sensory neurons of dorsal root ganglia at both synaptic and non-synaptic sites.[22] TREK-2 was found to be abundant in human kidney, pancreas, GI-tract and overlapped to the brain region where TREK-1 is present as well. Concerning the TRAAK

channel, it was observed to be largely and exclusively present in mouse, rat and human brain, overlapping TREK-1 and TREK-2 expression, confirming its potential role in the modulation of neuronal currents. However, the overlapping expressions of TREK channels in the same cells remain one of the main difficulties to assign currents to one or other channel. Many efforts have been done during the past years, in order to distinguish the ionic currents attributable to each cloned TREK isoform.

Since their discovery, several works were published and controversial results about TREK conduction emerged.[23] TREK-1 channel, for example, was found to have a voltage dependency detected by the cell-attached measurement of I-V relation, which exhibit an outward rectification under K^+ symmetrical conditions. Outward rectification was attributed to a voltage-dependent block of inward currents stimulated by the presence of extracellular Mg^{2+}. Due to the low probability of channel opening at negative membrane potentials, this behaviour was difficult to quantify, but Goldstein at al. demonstrated how the omission of Mg^{2+} ions in the extracellular side, selectively increased inward currents at negative potentials blocking the outward one, and influencing the voltage-gating activity.[23]

PKA-phosphorylation on the cytosolic C-terminal domain of TREK-1, was detected to be another factor able to influence gating modalities, producing Mg^{2+} analogous results. Specific analysis conducted in C-terminal domain deletion conditions (instead of N-terminal), demonstrated the crucial role for arachidonic acid (AA) and other lysophospholipids (LPC) activation for TREK-1.[24]

The typical background or “leak” activity of TREK-1 suggests that it influences both the resting membrane excitability and action potential duration. Many reports of direct interactions between general volatile anaesthetics and TREK-1 and TREK-2 have been published, such as chloroform, diethyl ether halothane and isoflurane.[25] They induce a channel opening favouring hyperpolarization of nervous cells and thus stimulating neuroprotection. Although neuronal pathways involved in such mechanism of anaesthesia are still not clear, it’s to date accepted that the opening of background K^+ channels would tent to depress neuronal excitability and could possibly play a key role in general anaesthesia[26,27].

TREK channels were discovered to have a central role in thermo- and mechano-sensation. Noel at al. have found that taken together TREK-1 and TRAAK channels act in controlling

the sensitivity in response to heat and cold.[28] Their main functions as temperature-sensitive is to serve as silencer partner of thermo-sensitive excitatory channels (TRPV1, TRPM8, etc.) in neurons. When they are open, they tend to suppress pain signal.[29]

For all these considerations, there is an increasing interest for new analgesic drugs able to modulate their functionality[30].

Another important evidence about unconventional modulation of conductance comes from Polyunsaturated Fatty Acids (PUFA) like Arachidonic Acid (AA). Many works have reported an ambiguous contribution to the conductance of TREK channels in the presence of increasing concentration of AA. The ambiguity resides in the lack of knowledge about the potentially direct (or not) implication of PUFAs molecules in the channel activation. This uncertainty is related to unrevealed interactions sites between AA and putative channel domains, which act as a gating sensor. Using chimeric mutant, Kim et al. have identified in the C-termini domains of TREK-2 and TRAAK, important sites for AA activation.[31] In particular, they showed how the replacement of the entire C-terminus with that of TASK-3 in a chimeric model preserves mechano-sensitivity, to the detriment of a direct free fatty acids activation. This evidence indicates that activation by AA and membrane swelling most likely involves a distinct molecular mechanism (Figure 6).

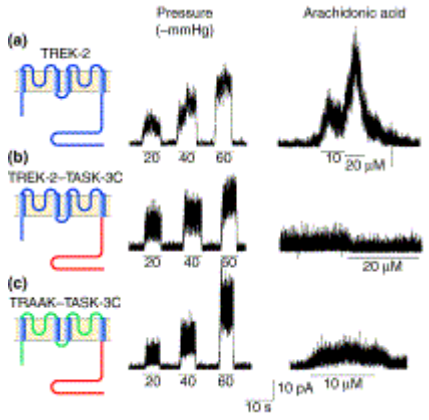

Figure 6. K2P channel currents recorded varying the experimental assay (negative pressure applied -left- with AA perfusion -right**)**

In contrast, analogous experiments were conducted on TRAAK channel in which C-terminus was once more replaced by TASK-1 and TASK-3 , showing that the sensitivities of this

mutant to free fatty acids, alkaline pH and membrane stretch are the same as wild-type TRAAK[31].

Again, their role was supposed to reside in the protection of cell damage activating outward currents and hyperpolarizing membrane cells, when AA concentration tend to rise during an inflammation event.

1.4 Membrane stretch activation: experimental evidences

As it was introduced above, among stimuli which play a role in TREK channels activation, lipids and membrane deformation (poking, swelling, fluid jet stimulation, pressure-induced stretch) are still matter of debate. In particular, the physical basis of mechano-sensitivity of TRAAK and TREK-1/-2 still remain to be well clarified. Despite the importance of electrophysiology in providing relevant information on macroscopic observables like channel currents, the atomistic details about channel-membrane lipids interactions are still elusive. These, however, can be in principle predicted and then analysed using Molecular Dynamics simulations (MD).[32] In this direction many efforts have been done in the past ten years, using both experimental and theoretical approaches, with the aim to understand the basis of transduction of membrane stretching to the channel gating. The mechano-transduction could be considered one of the oldest sensory transduction processes in living organism. Katz, Lowenstein and others, have been the firsts researchers which theorised the presence of specialized molecular switches, able to convert mechanical force exerted on cells membranes to electrical signals.[33]

Brohawn suggests three main different ways of membrane force-transmission to the channel.[34] The direct mechanism in which the force produced by a specific stimulus is directly transmitted by the surrounding lipids and then to the protein. Direct membrane-mediated gating can occur if a force induces tension in cell membrane, which can create a tension-dependent energy difference between the close and the open state. The second mechanism is related to the presence of accessory proteins able to transmit the stimulus signal to the channel. According to the third way, force from a stimulus works through upstream mechanosensitive molecule which initiates an intracellular signalling cascade

able to turn the channel on, to the ion conduction. Considering the rapid response to the electrical impulse for K2P channels (no delayed is detected during patch-clamp experiments, Figure2B), the first mechanism is more likely to be involved in the regulation of these channels. Regarding to this, through records of whole cell and single channel conductance of TREK-1 in rat cardiomyocytes, Li et al. found an increased current when negative or positive membrane pressure are applied respectively. Applying a 5µm stretch, i.e. increasing the distance between stylus and patch pipette, in whole cells recordings, increased current of stretch-activated K^+ channel in depolarizing condition (+60 mV) by ≈200 pA (Figure 7) were recorded.[35]

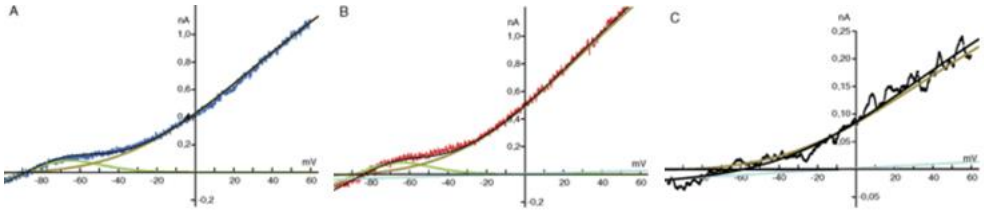

Figure 7. Recorded I-V curves in normal membrane conditions (A, blue trace) in Stretch conditions (B, red trace) and subtracting trace (C, black line).

Further analysis on single channel conductance in inside-out and outside-out patch-clamp were conducted to better identify the channel open probability (P_0) under membrane stretching condition.[35] In the single channel recording, an isolated channel is used to study individual ionic currents produced during a voltage-clamp; an hollow glass tube known as a *micropipette* filled with a specific electrolyte solution and a recording electrode is in direct contact with the membrane of an isolate cell (whole cell recording). From this configuration, in order to obtain a single channel patch, the *micropipette* is gently detached from the cell, and the cytosolic surface of the membrane (and thus the intracellular side of the channel) is exposed to the external bath (inside-out configuration). In this condition, the micropipette internal media correspond to the extracellular environment, whereas the bath the cytoplasmic one. In the opposite configuration, reached by an analogous procedure which does not intersect the channel at the starting whole cell configuration, the outside-out patch-clamp is obtained; in this case the intracellular environment is located inside the micropipette (Figure 8).

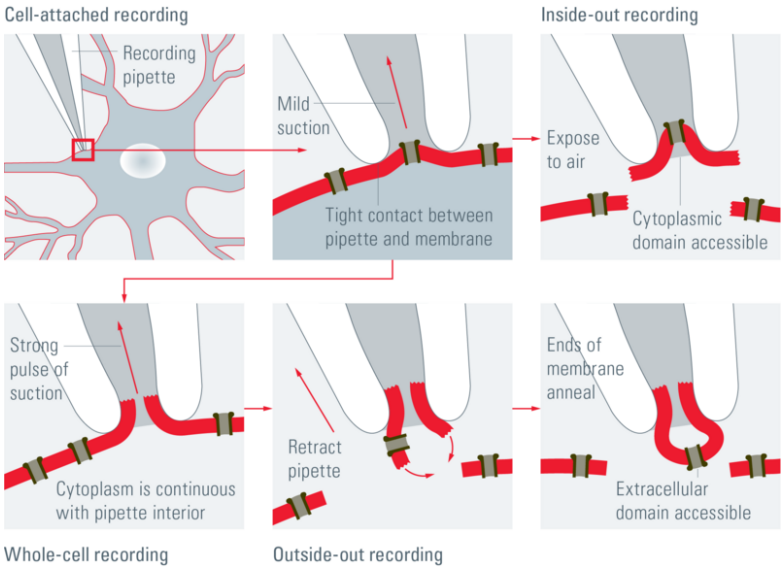

Figure 8. Illustration of a patch-clamp configurations

The alteration of the hydrostatic pressure applied to the patch pipette in inside-out or outside-out patch, produce as a direct consequence an elongation of the double leaflet in with the channel is embedded. Thanks to this experimental assay, important feature of the investigated channels can be highlighted, especially given by the alteration of the channel behaviour and so the measured currents.

Exploiting this framework, Li recorded for TREK-1 channel, the K2P typical conduction kinetic called "flickery and burst" where fast and alternate activation and deactivation events occurs. An increased number of channel opening events (NP_0 ≈27) was observed when the application of negative pressure in the inside-out recordings were performed, whereas application of positive pressure had no effect. Similar results were obtained (NP_0 ≈3) in outside-out experiment, when positive pressure was applied (Figure 9), suggesting that TREK-1 channel was activated by convex membrane curvature.

Similar results in slightly equivalent conditions of membrane stretching, were obtained by Brohawn et al., when currents were measured by hTRAAK single channel conductance.

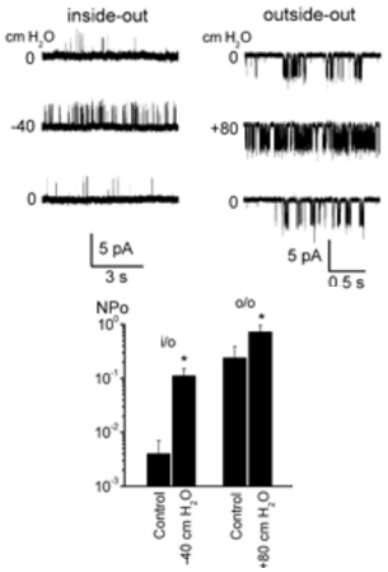

Figure 9. A) Inside-out (left) and outside-out (right) recordings at membrane equilibrium (upper trace), under membrane pressure (middle trace) and again at original conditions (lower traces). B) Histograms of channel opening probability (NP_0) in equilibrium and stretched conditions.

1.5 hTRAAK: a stretch activated K^+ channel

The third member of the TREK family besides TREK-1 and TREK-2, the human TRAAK channel was identified for the first time by Maingret et al. in 1999.[36] In this early work, experimentalists were able to localize high levels of expression in the central nervous system (brain, retina and spinal cord), specifically in the olfactory system, cerebral cortex, basal ganglia and cerebellum. Although a relatively low sequence identity with TREK-1 (less than 25%), TRAAK channel shared a similar membrane topology:

- Four spanning TM α-helix and two pore domains existing in tandem for each monomer
- Dimeric assembling
- Cysteine residue in the extracellular loop involved in disulphide-bridged homodimerization site
- High Selectivity for potassium ions

As well as other TREK channels, similar behaviour was recorded in physiological condition:

- Small outward current at negative potential in physiological [K^+]

- Ohmic trend of I-V curves in symmetrical [K^+]
- PUFAs and membrane stretching activation

In their study, Maingret et al. demonstrated that hTRAAK channel is mechanically opened, as well as TREK-1, by negative and positive pressures applied during inside-out and outside-out configuration respectively, suggesting that the channel is selectively activated by a membrane convex curvature.

In this first report, the authors were also able to characterize outward currents activated by perfusion of AA during voltage-clamp experiment. At first, the C-terminus domain (the most conserved region with TREK-1) was supposed to be essential to the AA channel activation. Nevertheless, same kind of results about hTRAAK conduction where obtained by Brohawn et al. in a truncated structure where the C-terminus domain was absent.[21] In fact, the extent of activation by AA above basal levels, was comparable to that measured from the full-length channel (Figure 10).

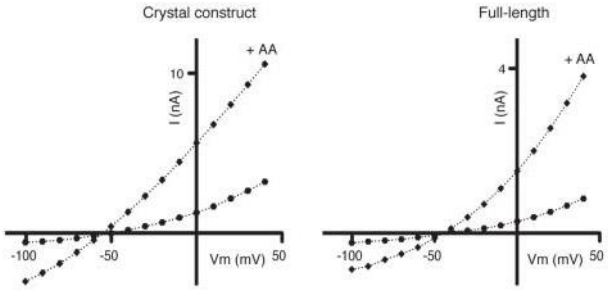

Figure 10.TRAAK IV curves measured from truncated channel (left) and full-length channel (right) in presence and absence of AA (adapted from ref.[37])

The truncated structure of hTRAAK channel was crystallized for the first time in 2012,[17] giving new insight about structural/functional characteristics, but important considerations have been made in 2014 when a second set of crystals were released by the same authors.[21]

The originally truncated structure (where the unstructured intracellular C-terminal domain was lost from Gln^{300}, PDB code 3UM7) was expressed and purified from *Pichia pastoris.* It was made by 255 residues from each monomer, and only two mutations were found in the N-glycosylation sites: N104Q and N108Q. Viewed from the bilayer plane, the N-terminal

domain is arranged in an α-helix motif, starting from the intracellular up to the extracellular side forming the first outer transmembrane (TM1) helix. In the extracellular side, the extension of TM1 is then packed to form a subunit called helical cap, extended ≈35Å above the lipid plane. Here a Cysteine residue located on the cap apex (one for each monomer) is involved in an inter-monomer disulphide-bridge. The helical cap domain is then linked to the pore helix 1 (PH1) which precedes the first pore loop (P-LOOP1, Figure 10). The first connection between P-LOOP1 and TM2, is formed by a loop which runs parallel to the membrane leaflet in the extracellular side. TM2 inner helix is largely composed by hydrophobic residues, which are in direct contact with the double leaflet, running diagonally along the membrane from the extracellular to the intracellular side. An important site where the helix starts to kink and run away down to the cytoplasm is represented by Gly165, a conserved residue traceable in every K2P channel. TM2 is linked by a small turn to the first helix of the second pore domain: TM3. Approximatively long as the TM1, TM3 is linked to PH2 by a two residues long loop. Unlike PH1, Pore Helix 2 (PH2) precedes the second P-LOOP(2), which runs approximately for 15 Å parallel to the ions conduction pathway. Again, one long loop link P-LOOP2 to TM4, which close the second pore domain up to the C-terminus in the cytoplasmic side (Figure 10).

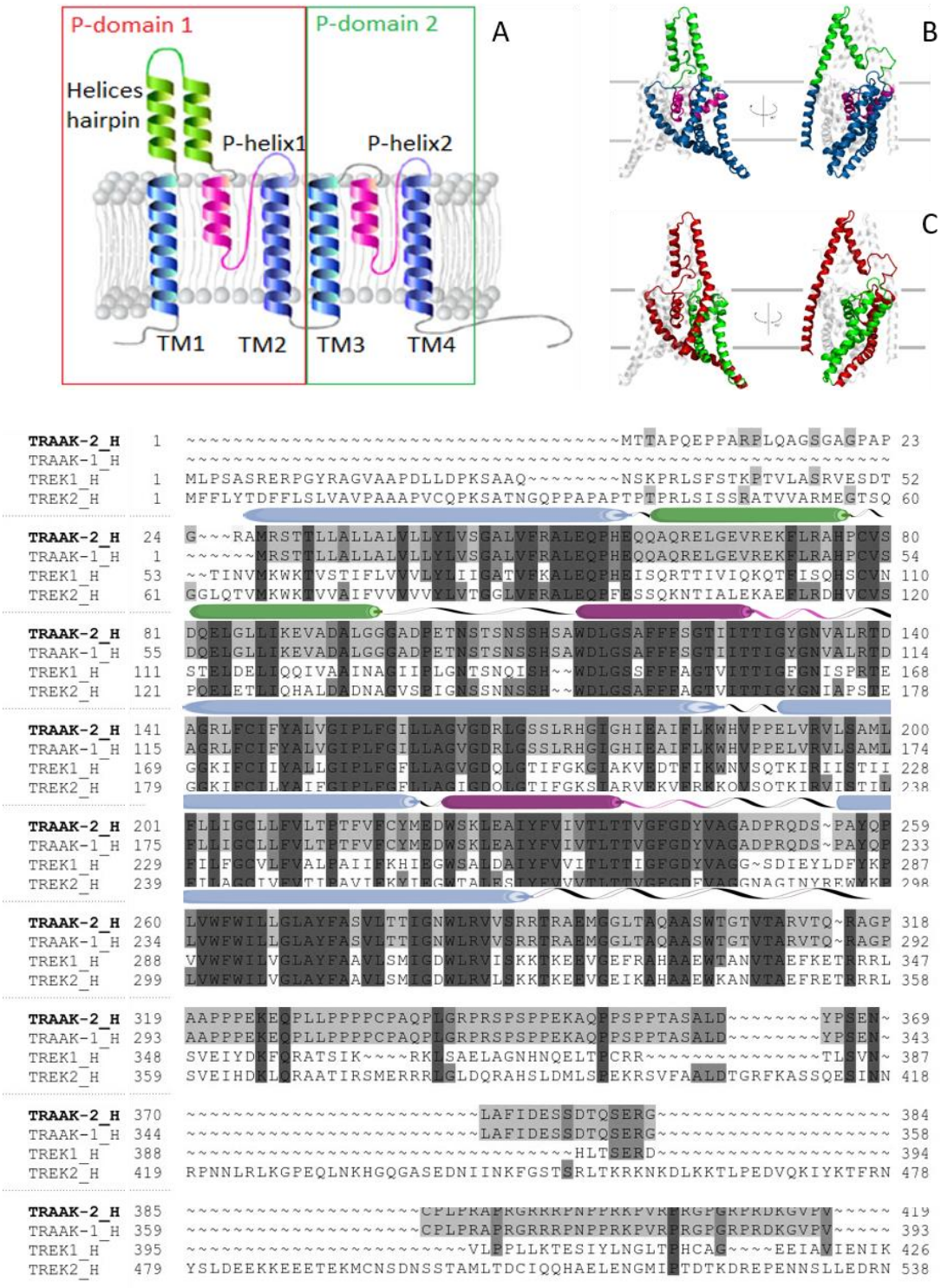

Figure 11. Schematic representation of a TRAAK monomer. a) 2D cartoon representation from the bilayer plane b) 3D representation of hTRAAK, coloured according to the 2D picture. In blue the four transmembrane helices, in green the two small outer helices assembled to form the helical cap, in pink the two P-helices and P-LOOPs c) 3D representation of asymmetric pore domains 1 and 2 (red and green coloured respectively). Below the alignment between hTRAAK isoform2, hTRAAK isoform1, hTREK-1 and hTREK-2

In contrast to the archetypal K^+ channel structures (KcsA), TRAAK has multiple regions characterized by a large asymmetry between pore domain 1 and 2. First of all, the presence of the two small outer helices folded to form the helical cap limited at the P-domain 1 only. The P-LOOP1 is connected by a 5 residues long loop to the PH1 and show an interaction network conserved in many K^+ channels, whereas the equivalent portion in P-domain 2 is double longer. Also, the SF shows asymmetry looking at the P-LOOP residual composition, which will be discuss below.

1.6 Conserved domain: the Selectivity Filter

Although the hypothesis of specific selection of potassium ions through a channel was theorised years before its discovery, the selectivity filter (SF, Figure 12) was observed for the first time in the 1998 thanks to the efforts made by MacKinnon et al.[12] SF is that portion where the catalytic activity is performed. Essentially, due to the geometry adopted by the main chain oxygens in the P-LOOPs, the pore is comprised of four domains faced and flanked each other, which identify four consecutive coordination shells constituted by five equally spaced carbonyl oxygens, arranged in a planar squared fashion.

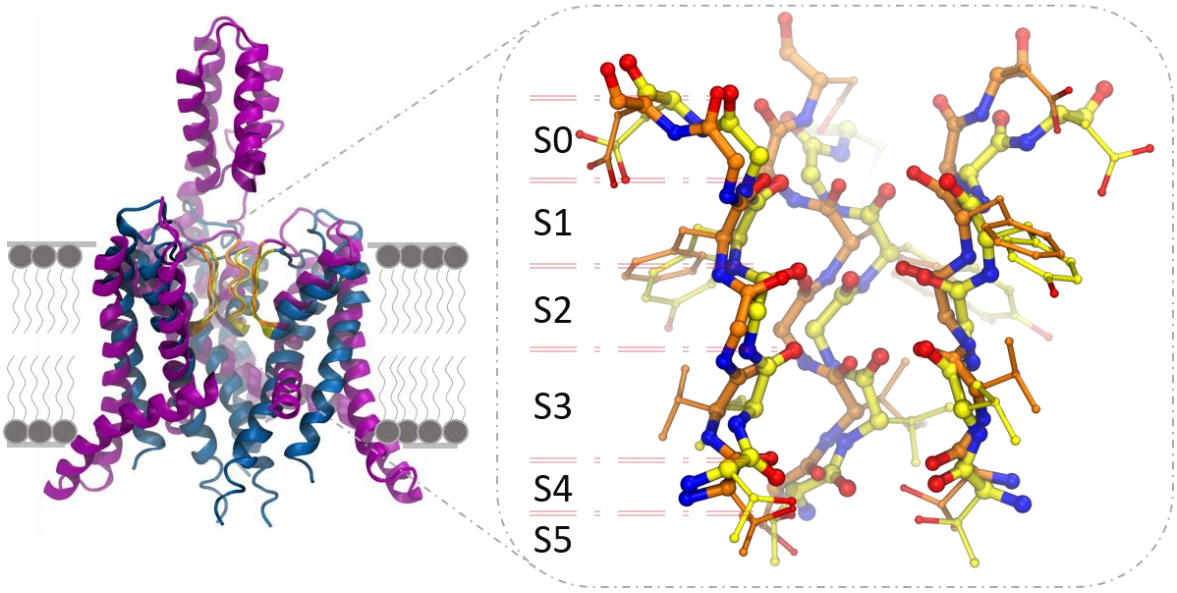

Figure 12. KcsA prototypical protein (Pore domains, blue) superimposed to hTRAAK (purple). Focus on Selectivity filter side view of KcsA-SF and hTRAAK-SF (coloured in yellow and orange respectively). Coordinative slots of the pore domain (rangeing from S0 in the extracellular to S5 in the intracellular side) are shown.

The approximatively evenly spaced distance (≈ 3.0 Å) between each oxygens plane, form a coordinative channel slot. From the top of the SF, S1 to S4 coordinating cages run for ≈ 12 Å, whereas ≈ 2.5 Å is the diameter. Each slot is made by eight carbonyl oxygen atoms, which adopt an antiprismatic geometry able to interact and sequentially coordinating those ions that pass through it during the translocation. Other two semi-coordinative positions are located at the intracellular entrance (IC, S5) and at the extracellular one (EC, S0), in the region where the ion desolvation/solvation process occurs. As previously mentioned, the SF domain is highly conserved, mainly formed by TXGYG pentapeptidic sequence. From the crystal structure 1K4C[38] where the protein is fully loaded by K^+ ions within the SF, it was possible to calculate the coordination distance O-K, which is demonstrated to range between 2.7 to 3.1 Å, quite close to the theoretical water coordination diameter (2.8 Å).[38] The selectivity of K^+ ions is mainly due to the ionic size. Considering the difference between potassium and sodium ions (0.4 Å) the coordination of the smaller one was in principle supposed to be unfavourable. This hypothesis was formulated looking at the geometrical feature of KcsA crystal structure, but was later confirmed by Bucher et al.[39] Using molecular dynamics simulations (MD) and hybrid quantum mechanical/molecular mechanics

calculation (QM/MM) they calculated the theoretical dimensions of the coordination shell (and so the average number of coordinating oxygen atoms) of K^+ ions, comparing them to the Na^+ ones both in the SF and bulk water.

Table 1. The average coordination number of K^+ and Na^+ cations by water molecules calculated through MD and QM/MM methods, compared to Experimental values. In the table are also shown the average number of water molecules within the SF.

Average Coordination Number

	K^+	Na^+
Bulk Water		
MD	6.6	5.3
QM/MM	6.2	5
Exp.	5.9 - 6.4	4.4 - 5.4
Selectivity Filter		
MD	6.7	6.0
QM/MM	6.6	5.3

Observing the radial distribution functions, and calculating the relative numbers of coordinating water molecules (Table 1), by using different computational approaches, they concluded that the coordination of a smaller atoms, had an impact on the distances between opposite oxygens in the SF planes. As smaller the distance between oxygens, as higher the carbonyl repulsion, which causes a more difficult coordination for Na^+ and thus a K^+ selection.[39]

If the selectivity within the SF could be considered strongly dependent by ionic radius, the same cannot be said for water molecules. Indeed, the scientific community is still debating about their possible role on the filtration and activation/deactivation/inactivation transition, although no crystal structure was found with water within the pore.

The SF domain is certainly the most conserved portion shared by K^+ channels. As was stressed above, the majority of potassium channels bears the characteristic four-folded shape where identical subunits are assembled to create the catalytic domain.[1] Usually, the SF is a symmetrical domain composed by: Thr-X-Gly-Tyr-Gly-Asp, where X is typically a

hydrophobic residue. In hTRAAK, this symmetry is broken because of two main features: two pore domains are included on each subunit (chain A and B), and P-domains are constitutively different.

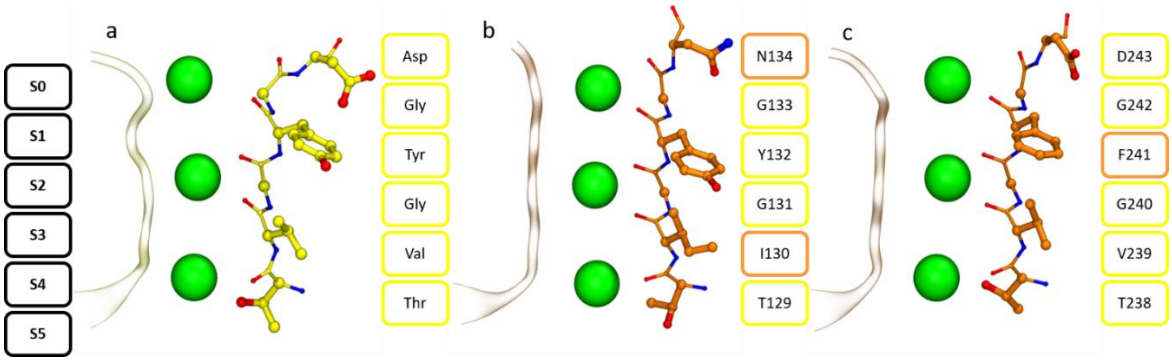

Figure 13. Sequence asymmetry between prototypical KcsA-SF and TRAAK-SF partially loaded of K^+ ions located in S0, S2, S4 coordinative slots. a) KcsA P-LOOP b) TRAAK P-LOOP of P-domain 1 c) TRAAK P-LOOP of P-domain 2.

A comparison between hTRAAK and KcsA (Figure 12 and Figure 13) demonstrates that the overall two-fold symmetric channel converges to a four-fold symmetric pore helix and SF. In the homotetrameric KcsA a symmetric pore is formed, whereas in hTRAAK two domains, 105 residues distant each other, show sequence diversity, concurring to form the same catalytic site. The main differences between the canonical sequence of KcsA and the hTRAAK P domains 1 and 2, are related to those residues located in S0, S2 and S4 positions (Asn134 in P-LOOP1 instead of Asp in KcsA and P-LOOP2; Phe241 in P-LOOP2 instead Tyr in KcsA and P-LOOP1; Ile130 in P-LOOP1 instead of Val in KcsA).

The literature regarding the dynamical behaviour of SF in K^+ channels, is dense of studies reporting on the activation and inactivation processes. Indeed, many reports have identified in the SF backside, where the sidechains are oriented away from the pore, a region in which the C-type activation (or inactivation) could start. Cordero-Morales et al. for example showed how the limited flexibility of the aspartate side chain of the S0 site in KcsA, could restrict the conductive state because unfavourable interactions with adjacent P-helix residues.[40]

Other theoretical studies regarding simulation and analysis of the H-bond interactions between SF-sidechains and P-helices respectively bridged by water molecules, were conducted. Domene et al, gave new evidences about the key role of the interdomain region hydration, next to the pore and the stabilization of conductive SF conformation in KcsA.[41]
An important focus on the SF flexibility of K2P channels, was recently published by Oakes et al: they were able to simulate a large number of conformation adopted by SF as a function of intrinsically different interactions between P-helices and P-LOOPs in TWIK-1 channel[42]. Like other K2P channels (and hTRAAK among them), P-LOOP 1 and 2 differ from each other and also from the KcsA canonical sequence. Comparing TWIK-1's P-LOOP1 and KcsA canonical sequences, Histidine residue was found to be located at the entrance of SF (S0) instead of an Aspartate, and the hydrophilic Threonine in S3 substitutes the Valine residue in the equivalent position, maintaining an high identity for the rest of sequence. In P-LOOP2 Leucine and Isoleucine replaced Tyrosine in S1 and Valine in S3 respectively. They proposed that the variability of SF sequences has an impact on the K^+ ions conduction within the pore, mainly due to the protonation state of His122 in P-LOOP1 (and the related H-bonds waters network), revealing a putative pH-modulation site of ion conduction.

1.7 Proposed gating mechanism: TM4 displacement

A further important and possibly functional source of asymmetry found in hTRAAK, comes from the displaced conformation adopted by the TM4 helices of each subunit. Their conformations have been well characterized in the second set of crystals released in 2014 by Brohawn et al., in which the protein adopted two different putative open and closed states. These states have been correlated to the channel functionality.[21]
hTRAAK was crystallized in complex with Fabs monoclonal antibodies at 2.5 Å resolution, in presence of decyl maltoside detergent and 150mM [K^+] salt. The so obtained crystal (PDB code: 4WFF) revealed an asymmetric orientation of the two TM4 helices. The TM4 from the subunit A was found to interact with the proximal side chain residues of TM2B helix in a conformation called "up", creating a continuous protein surface able to prevent membrane lipid access to the protein gorge. The conformation of TM4B was significantly

displaced compared to the same domain of A subunit, adopting the so called “down” conformation, where the distance between two transmembrane helices (TM4B-TM2A) is increased of ≈4.5 Å. Around a pivotal conserved residue (Gly268), TM4B adopts a tilted conformation of ≈15° (along the projected helix axes) diverse from the TM4A. The intramembrane opening between subunits creates a fenestration that exposes the channel cavity to the inner leaflet lipids. This atypical asymmetric conformation was maintained because of the presence of a co-purified ten carbon long acyl chain. The authors have interpreted the obtained crystallographic data consistently with the hypothesis of a further molecule able to interact with hydrophobic residues along the TM4/TM2 helices, like a hypothetical membrane lipid. To demonstrate this hypothesis, they crystallized once more hTRAAK using almost the same experimental conditions, replacing K^+ ions with an equimolar [Tl^+], and again the conformation adopted by transmembrane helices resulted “up/down” (Figure 14-A, left).

The lipid located at the entrance of the channel pore, from the cytoplasmic side, was proposed to act as a blocker of the ionic flow obstructing the access. Possibly, it gives a contribution to an increased hydrophobicity of the channel gorge. The hypothesis of protein lipid interactions along the cavity surface, acting as a promoter for conformational changes, where the lipid aliphatic tail is able to fall down in the ionic pathway, was already theorized in previous studies.[43] Results consistent with this observations where obtained through MD simulations of TWIK-1 channel performed by Aryal et al. TWIK-1 was simulated in a membrane double leaflet of 1-palmitoyl-2-oleoyl-sn-glycero-3-phosphocholine (POPC) lipids, and was found to have an hydrophobic gate at the channel entrance. The researchers focused their attention on the proteins intramembrane surfaces domains and lipid distribution around it, monitoring the lipids residence time inside the channel, concluding that terminal carbon of surrounding tails from the lower leaflet can penetrate the fenestration between protein subunits, contributing to the conformation of the inner cavity.[43] Although they conclude that only long lipid tails (e.g. > 24 carbon) might be able to directly occlude the pore (and this should be a more general characteristic and not only related to lipid-TWIK-1 interactions), in the “up/down” crystal of hTRAAK provided by Brohawn, there is an experimental evidence of such kind of lipid lock.

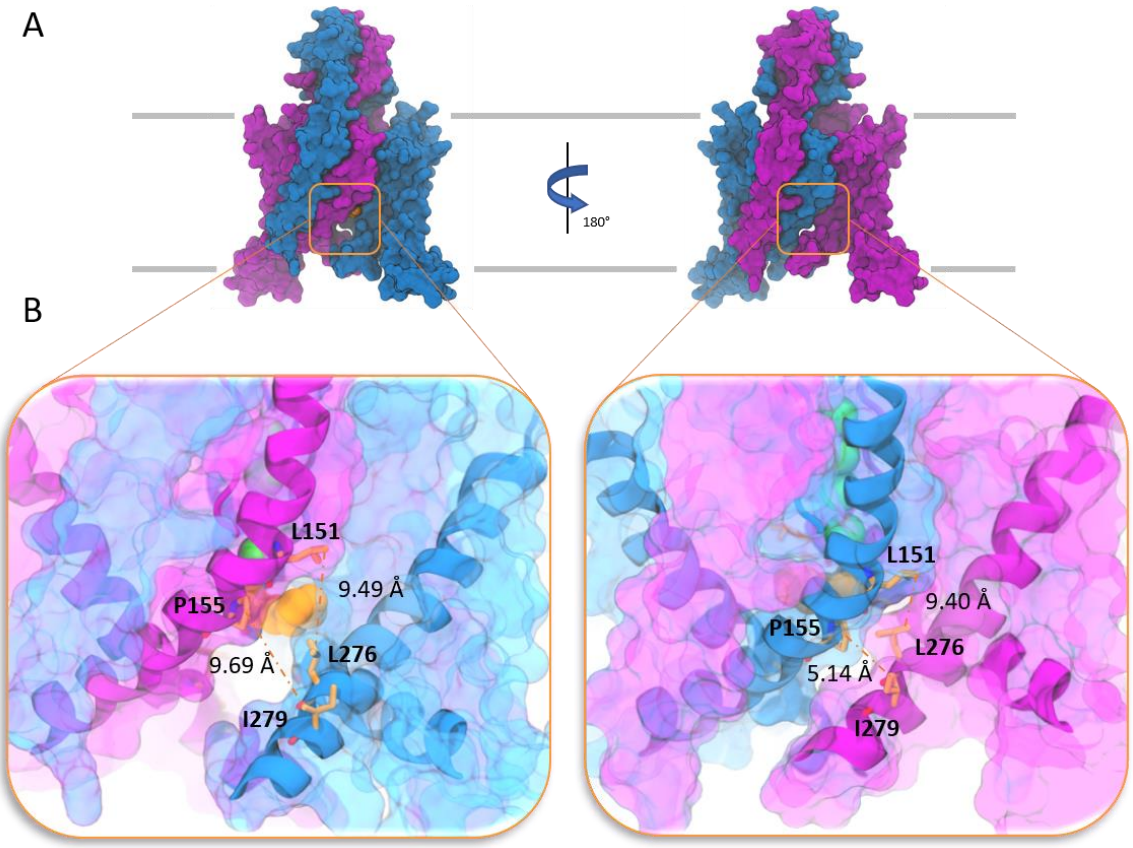

Figure 14. Pictorial illustration of hTRAAK (PDB code 4WFF) channel in asymmetric conformation. A) Representation of channel surfaces, from membrane side view. On the left side the "up/down" conformation; on the right side the "up/up". B) Details of putative lipid blockage, performed by the aliphatic tail of a co-crystallized molecule (decyl-maltoside, orange spheres). The side opening between TM4 and TM2, is shown on the left, and monitored by the distance between key residues (showed in orange stick)

The hypothesis of an up/down conformation related to the protein nonconductive state was further investigated by mutagenesis experiments. The authors were able to mutate two hydrophobic residues located along both the TM4 and TM2 helices with Cysteine residues (I159C, R284C), testing the protein conduction as a function of oxidizing/reducing conditions. Oxidized (thus disulphide bonded) cysteine residues localized on the two faced TM4B-TM2A, allows the side opening fenestrations closing, preventing the lipid access and maintaining the "up/up" conformation . With both intramembrane openings sealed, TRAAK mutant was rapidly activated, suggesting that the formation of a disulphide bridge stabilizes a conductive conformation. On the other hand, measured currents of reduced mutant TRAAK were significantly lowered (Figure 15).

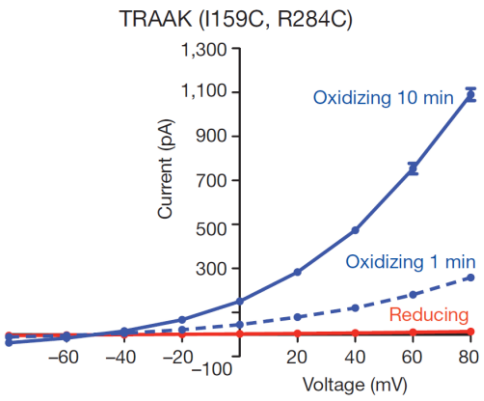

Figure 15. Outwards current mesured by patch clamp experiments in oxidizing (blue), reducing (red) condition of mutaded hTRAAK.

These data appear to confirm the hypothesis of a sealed up/up conformation of both TM4 seems to be more active than the “free to move” not linked one, but regarding the putative lipid blockage no more details come from this analysis.

Intimate interactions between TM4 and the TM2/TM3 in the intracellular side revealed by crystals, give rise to the idea of a stretch sensor located on the fluctuant helices (TM4s). There is the suspect that they could be able to follow the protein enlargement during a membrane stretching, which is well known to be an activating impulse for K^+ transport in hTRAAK. What is seems to be certain is that the TM4-mediated gating mechanism contribute to the channel activation, but the key interactions between this new putative protein sensor and channel activation are still unknown.

Aim of the Study

K2Ps are an important class of potassium channels, mainly involved in the regulatory mechanism of electrical signalling in nervous system. Because of their central role in regulating the action potential of excitable cells by restoring/maintaining the resting potential, understanding their functionality is of primary importance in biophysical research. Moreover, the recent discovery of their implication in several diseases has raised the attention on these channels as potential drug targets. In particular, the hTRAAK channel (belonging to the TREK family), has been suggested to play an important role in neuroprotection. While it is nowadays clear that this cannel responds to several physical (temperature, membrane swelling) and chemical (pH, anaesthetics, arachidonic acid) stimuli, a detailed interpretation of the mechanisms implicated in its functionality is still missing.

Molecular dynamics (MD) simulations represent a powerful tool to investigate molecular processes at an atomistic level of detail. Thanks to recent advances in hardware and software, microsecond-long simulations can be systematically performed for systems comprising several hundreds of thousand atoms. However, even within this regime of high-performance computational power, MD simulations are still suffering from severe limitations. First, sampling biologically relevant events remains a challenge, and this is particularly relevant whenever the investigated process takes place on timescales that exceed what is currently affordable with simulations. Second, the commonly adopted modelling setups (including equilibrium conditions, periodic boundary conditions, and treatment of long-range electrostatics) are strongly limiting the realism required to reproduce specific experimental conditions. For example, membrane stretching is not usually modelled, nor the physiological concentration of ions in the two sides of the membrane can be achieved through conventional setups.

In this thesis, we employ enhanced sampling methods and dedicated modelling setups in order to overcome these main limitations. In particular, we apply these methodologies to investigate some peculiar aspects of the polymodal activity of hTRAAK.

2 Materials & Methods

2.0 Proteins preparation

The protein structural models for the simulations were taken from the experimental crystallographic structures accessible at the PDB codes 4WFE, 4WFG (TM4s up/up conf.), and 4I9W, 4WFF (TM4s up/down conf.).[21,44] Missing residues belonging to the unstructured C-terminal and N-terminal domains were not modelled, thus starting and ending residues were Arg28 and Arg284, respectively. Acetyl- and N-Methyl- (ACE and NME) groups were added in correspondence of N-terminus and C-terminus, respectively. Missing gaps connecting the helical cap to the PH1 were modelled using Schrödinger 2015-2 Prime:[45] hexa-peptide gap on chain A Gln104-Ser105-Thr106-Ser107-Gln108-Ser109 and tetra-peptide gap on chain B Thr106-Ser107-Gln108-Ser109 were rebuilt. The Cysteine residues (Cys68) located in the helical cap, were oxidized to form a disulphide bond. The initial structures were composed by 256 residues per chain.

The Ca^{2+} ion found in the X-ray structure as well as the K^+ and Tl^+ within the selectivity filter and Fab antibody were removed from all the crystallographic water molecules interacting with the external moiety of SF and hydrophilic helical cap were maintained. Initial guesses for missing hydrogens and ambiguous protonation states have been evaluated through Schrödinger 2015-2 Protein Preparation Wizard[46] and chosen after a visual inspection. All histidine residues were protonated on the epsilon nitrogen atom.

2.1 Lipid occlusion investigation: MD simulation setup

2.1.0 Protein embedding and solvation

Only one of the four protonated proteins (TM4s up/down conformer, PDB code 4I9W) was selected to investigate the lipid occlusion. It was oriented along the *z*-axis through VMD 1.9.3[47] Orient tool in order to be embedded on a purposely oriented (on the *xy*-plane of the simulation box) 1-palmitoyl-2-oleoyl-sn-glycero-3-phosphocholine (POPC) membrane.

The protein embedding was performed by means of a procedure implemented in BiKi Life Sciences[48], which used a pre-equilibrated membrane of 356 POPC lipids. The so-obtained complex was then solvated accordingly (by using the VMD plug-in SOLVATE 1.0), leading to a cubic simulation box of approximately 110 Å per size for a total amount of 140,000 atoms. The simulating system was then neutralized and ionized by adding a symmetrical KCl concentration of approximately 150 mM, and electroneutrality was reached. K^+ ions were manually positioned to the S5, S3, S1 coordinating shells of the SF, and kept in place throughout the simulations using positional restraint (100 kJ/mol/ $Å^2$ force constant). Water molecules were placed in the SF sites S2 and S4.

2.1.1 Plain molecular dynamics simulations setup

NAMD-2.10[49] was initially used to run plain MD simulation (**run-4i9w-lip**). The CHARMM36[50] force field was adopted to treat protein and lipids. The simulations were carried out in the isothermal-isobaric ensemble at the temperature of 300 K and pressure of 1 bar. Langevin dynamics was performed using a damping coefficient of 5 ps^{-1} and with a uniform integration step of 2 fs. The pressure was controlled with the Langevin piston[51] implemented by NAMD, applying a semi-isotropic pressure coupling. Bonds involving hydrogen atoms were restrained to their equilibrium values with the SHAKE algorithm[52]. Short-range non-bonded interactions were treated with a cutoff of 12 Å with a switching function active at distances larger than 10 Å. The nearest neighbor search was performed within a radius of 14 Å, and the list was updated each 10 integration steps. Periodic boundary conditions were adopted, and long-range electrostatics was accounted for with the PME method[53] using a grid spacing of less than 1 Å in every dimension, and a fourth-order spline interpolation scheme.

The system was minimized for 1,000 steps using a conjugate gradient scheme and then heated up to the target temperature in three steps in the NVT ensemble. Simulations were run for 150 ps each, with an integration time step of 1 fs. All lipids and protein heavy atoms and K^+ within the SF (K^+_{SF}) were harmonically restrained with a force constant of 1000 kJ/mol/$Å^2$. The system was equilibrated in two further stages for 0.5 and 1 ns respectively

with an increased time step (2 fs), in the presence of protein Cα atoms/K^+_{SF} restraint and SF Cα atoms/K^+_{SF}, respectively at 1000 kJ/mol/Å^2.

The equilibration phase has been concluded switching to the NPT ensemble (and using the parameters reported above) in three different stages and relaxing protein and lipids restraint. The final system was simulated in the presence of K^+_{SF} atoms restrained with a force constant of 100 kJ/mol/ Å^2 for 500 ns. The trajectory was analysed by using of the *driver* tool of PLUMED2.3b[54] and three selected frames, in which relevant interactions between occluding lipid and the SF were observed. Those three snapshot have been extracted, further investigated, and used as initial point of enhanced sampling simulations like Well-Tempered Metadynamics (WTmetaD)[55].

2.1.2 WTmetaD: theory and setup

In computational biophysics, biased simulations are techniques developed with the aim to sample the low-probability regions of a Free Energy Surface (FES) associated to a molecular events. In this respect, Metadynamics[56] allow the computing of FE landscapes related to a specific reaction coordinate, allowing the acceleration of rare biophysical events along it. By adding small Gaussian-shaped potentials to the reaction coordinate every few simulation steps, the system is discouraged to remain trapped in local minima during the FES exploration, and is potentially forced to visit any available state. Stable configurations will be found in correspondence of energetic minima, and these will be filled by Gaussian-potentials, allowing the system to escape via the lowest transition state to the next stable state. The simulation time required to escape from a FES local minimum depend by the depth of the well (i.e. the stability of the considered configuration), and the number, the height and the width of added Gaussians. If small enough Gaussian are added at suitable intervals, the FES of the system under study will be accurately reconstructed. The chosen reaction coordinate is defined Collective Variable (CV), and is a differentiable function (let us call it $S(\chi)$) of atomic cartesian coordinates ($\boldsymbol{\chi}_i$, with *i* between 1 and *N*, the total number of atoms), used to reduce the number of degrees of freedom of the system.

In the original Metadynamics implementation,[57] the external history-dependent Gaussian potential *V* (function of the chosen CV; can be written as *V(S)*) is added to the system Hamiltonian *H* and is continuously updated at rate *ω*:

$$H = T + V + V(S) \quad ; \qquad \frac{\partial V(S)}{\partial t} = \omega\delta(|S - S_t|) \tag{1}$$

Which means that in an infinitely long simulation time, the accumulated bias potential converges to a free energy as a function of the CV, with opposite sign:

$$V(S,t) = \int_0^\infty \omega\delta(|S - S_t|)dt \qquad F(\vec{s}) = -\lim_{n\to\infty} V(S,t) + \mathrm{C} \tag{2}$$

The real form of bias potential is centered at the instantaneous collective variable values *S* at time *t*

$$V(S,t) = \int_0^t dt' \, \omega \exp\left(-\sum_{i=1}^{d} \frac{S_i(\chi) - S_i(\chi(t'))^2}{2\,\sigma_i^2}\right) \tag{3}$$

where *ω* is the energy rate and *σ* is the Gaussian width. The energy rate *ω* is constant and usually expressed in terms of Gaussian height (*W*) and deposition stride (τ_G).

$$\omega = \frac{W}{\tau_G} \tag{4}$$

Those are the parameter used to govern the Metadynamics. They need to be carefully chosen in order to obtain a balance between accuracy and sampling efficiency.

In the WTmetaD formalism[55], the initial deposition rate ω_0 of the bias potential decreases with the bias accumulated over time. This is achieved by rescaling the Gaussian height *W* according to:

$$W = \tau_G \omega \, e^{-\frac{V(S,t)}{k_B \Delta T}} \tag{5}$$

where *τ* is the gaussian potential deposition stride, ΔT a temperature and *V(S,t)* is the bias potential accumulated in the CV space over time *t*. At variance with standard Metadynamics, the bias potential does not fully compensate the Free-energy Surface (FES), but it converges to:

$$V(S, t \to \infty) = -\frac{\Delta T}{\Delta T + T} F(s) \tag{6}$$

where T is the temperature of the system. At convergence the CVs sampled at a (fictitious) higher temperature T + ΔT, with a probability distribution of the sampled events related to:

$$P(S, t \to \infty) \propto e^{-\frac{F(S)}{k_B(T+\Delta T)}} \quad (7)$$

WTmetaD was used to study the single K^+ translocation from the bulk solution to the SF entrance. As was previously introduced, three relevant configurations were extracted from the plain MD trajectory and used as starting point for biased simulations. In these three frames, a lipid was observed to obstruct and interact with the SF in a fashion similar to the one proposed by Brohawn et al.[21] In order to understand if the lipid occlusion had an impact on the K^+ translocation, two geometrical parameters were used as CSs: the projection of the *z* Cartesian coordinate of potassium ion along the channel axis and the distance from that axis. The aim was to identify possible barrier for ion permeation along the conduction pathway from bulk solution to the S5 coordinating shell, in the presence of an obstructing lipid. Actually, this lipid was found in the previous plain MD, to interact with the SF in three conformations (namely "tail-dangling", "head-occluded", "tail-occluded") Minimum and maximum values of Gaussian widths were set to 0.05 and 0.5 Å respectively, in both dimensions. The initial Gaussian height was set to 0.1 kcal mol^{-1} together with a bias factor of 10 units. The deposition stride was set to 1 picosecond.

The three WTmetaD simulations were conducted until the free energy was reasonably converged in the main basin, for 50 ns.

2.2 Membrane stretching investigation: MD simulations setup

2.2.0 Protein embedding and solvation

The embedding procedure was repeated starting from the orientation of the protein along the *z*-axis, using the VMD 1.9.3[47] Orient tool

The protein embedding was performed by means of a procedure implemented in BiKi Life Sciences[48], which used a pre-equilibrated membrane of 356 POPC lipids. The procedure

consist of a three steps phases: i) the first the superimposition between the oriented membrane and a scaled (literally shrunk) protein, was performed; ii) the second phase was needed to perform the lipid removal, generating a cylindrical hole within the membrane; iii) in the third phase, the protein was relaxed in order to restore the original dimensions minimizing lipid-protein interaction, preventing atomic clashes. The final membrane was constituted by 345 lipids.

The embedding procedure was performed three times for each conformer, in order to obtain multiple replicas of each system. Moreover, the protein orientation along the *z-axes* was changed time by time (rotated by an angle of 45°, Figure 16), to achieve different initial configurations of lipids around the channel.

Finally, the whole system was solvated using TIP3P model water molecules using VMD Solvate plug-in in a periodic rectangular box (sizes 110 X 110 X 150 Å). The ending step of the system preparation was the neutralization (the system had a net charge of -12) and ionization using Auto-ionize plug-in included in VMD; a final concentration of 150 mM of KCl and NaCl has been set, up to approximatively 181,000 atoms. Three K^+ ions were manually placed into the SF, giving a S0, S2, S4 configuration (Figure 16-inset)

Structure and topology files (PDB and PSF files) created by VMD were converted accordingly to GROMACS format. GROMACS 5.1.2 MD package[58] was used for conventional and biased (under stretching conditions) simulations. The force field used was CHARMM36ff[50] for lipids and proteins.

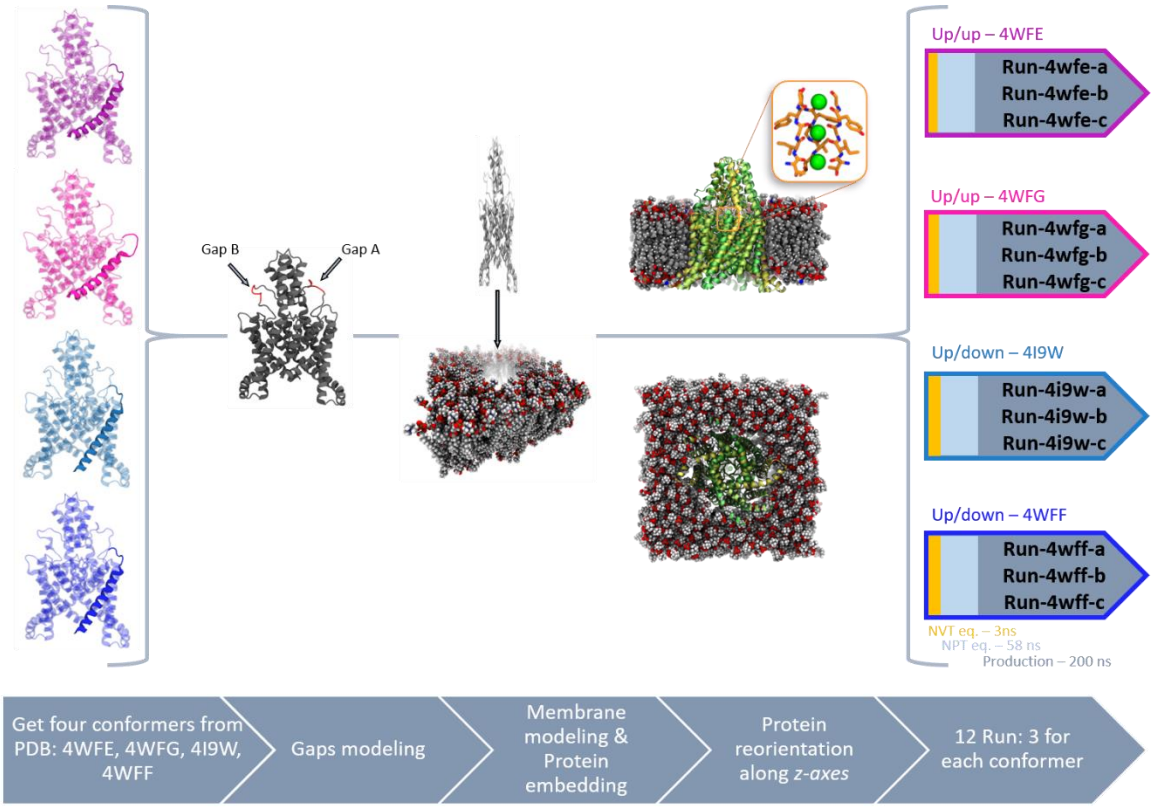

Figure 16. Schematic representation of the preparation setup, from the crystal (left), to the simulation runs (right).

2.2.1 Plain MD Simulations

The embedded, solvated, ionized complexes were simulated using GROMAC-5.1.2 MD engine. They have been minimized with 50,000 cycles of the steepest descent algorithm. Then, the system has been equilibrated in 5 different stages in NVT ensemble and 2 stages in NPT. Concerning the NVT ensemble, the V-rescale thermostat[59] was used with a relaxation time τ of 0.1 ps, to keep the system at the desired temperature. The temperature was increased up to 300 K in the first three heating stages. They were run for 150 ps each, with an integration time step of 1 fs, in the presence of all lipids and protein and K^+ within the SF (K^+_{SF}) heavy atoms harmonically restrained with a force constant of 1,000 kJ/mol/Å^2. In the last two stages, the simulation was run for 0.5 and 1 ns respectively with an increased time step (2 fs), in presence of protein Cα atoms/K^+_{SF} restraint and SF Cα atoms/K^+_{SF} respectively at 1,000 kJ/mol/Å^2. The NPT equilibration phase has been performed in three different stages using the follow parameters:

1) Parrinello-Raman barostat[60] (τ = 1 ps), reference pressure P = 1 bar, semi-isotropic scaling box vectors; thermostat was switched to the Nose-Hoover[61,62] with a time coupling τ of 1 ps, reference temperature of 300 K; restraint applied to backbone heavy atoms, and the simulation was run for 3 ns at 2 fs time step

2) all controlling pressure and temperature parameters were maintained, the restraint were applied to all Cα atoms and K^{+}_{SF}, time step of 2 fs for 5 ns

3) finally, the long equilibration stage in which only the restrained atoms where changed to K^{+}_{SF} at 1,000 kJ/mol/Å^2 force constant at 2 fs for 50 ns.

Concerning the pressure and temperature coupling the protein and the double leaflet were grouped together, as the bulk water and ions too. Bonds involving hydrogen atoms were restrained with the LINCS algorithm.[63] A short-range nonbonded cut-off of 1.2 Å was applied, whereas long-range electrostatics were treated with the particle mesh Ewald (PME) method[53] with a grid spacing of 0.16 Å. Periodic boundary conditions (PBC) were applied.

12 independent simulations were performed (**run-4wfe-a,b,c, run-4wfg-a,b,c, run-4i9w-a,b,c, run-4wff-a,b,c**) and each simulation runs for at least 200 ns. for a total of 2.4 μs.

The reliability of the force field and simulations parameters were validated by measuring the area per lipid, the order of lipid tails, and density profiles (Figure 17) and compared with experimental data.[64,65] The deuterium order parameter and membrane thickness were calculated using the analysis tools provided with GROMACS-5.1.2, and Area per Lipid (APL) was calculated using GridMat-MD utility.[66]

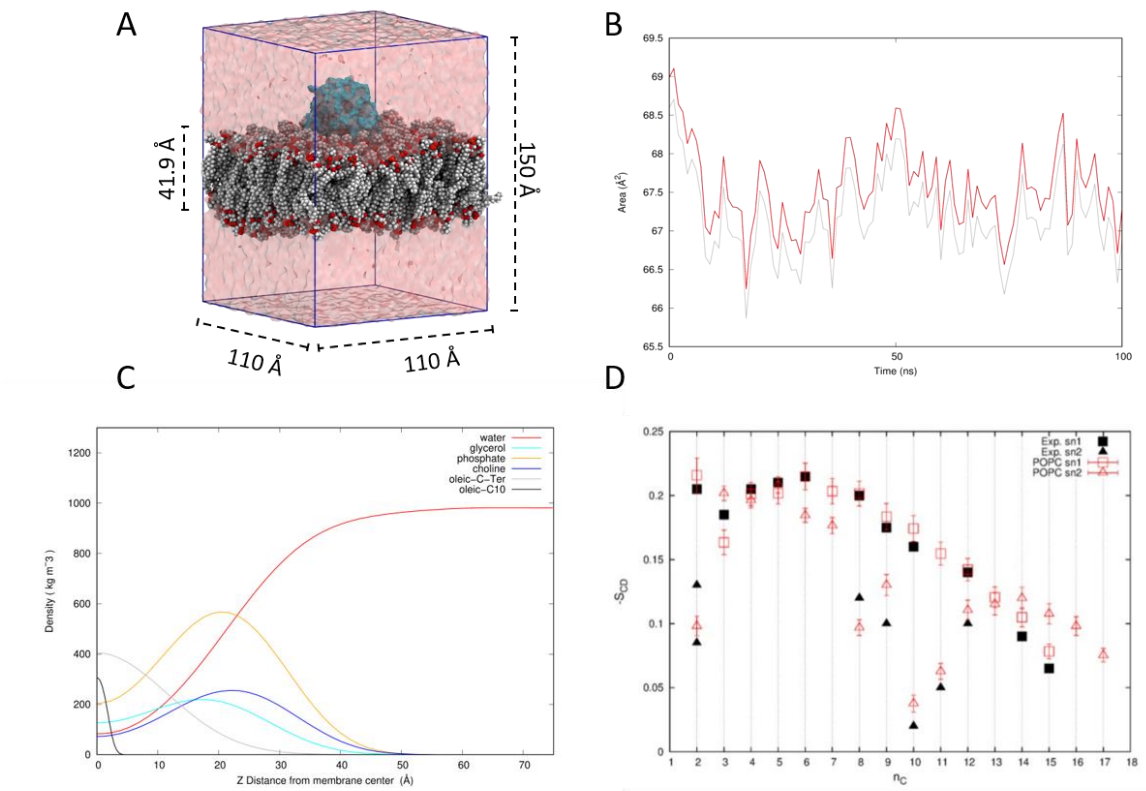

Figure 17. Representative parameters checked out to evaluate the membrane equilibration. A) Representation of the simulation box and its dimensions. B) Time evolution of APL parameter for the upper (red trace) and lower (grey trace) leaflets. C) Density distribution of the selected lipid atoms for the evaluation of membrane thickness. D) Distribution of deuterium order parameters S_{CD}.

2.2.2 MD Simulation in membrane stretching configurations

To further investigate the stretching-induced changes in hTRAAK, the ending structures obtained from the plain MD runs were used to perform a new set of 12 simulations (**run-4wfe-a,b,c-st, run-4wfg-a,b,c-st, run-4i9w-a,b,c-st, run-4wff-a,b,c-st**), in the presence of applied negative pressure to the *xy*-plane (membrane). GROMACS-5.1.2 was used.

The isothermal-isobaric ensemble (NPT) was used for all simulation. The bilayer plane pressure was varied from +1 to -50 bar, whereas the pressure in bilayer normal *z*-axis was kept at +1 bar. As in previous simulations constant temperature of 300 K has been set. The lateral pressure was applied exploiting a GROMCS functionality, which allow the user to set multiple independent values depending on the pressure coupling schemes; for these

simulations has been set to semi-isotropic, thus normal pressure ($P_\perp$) was independent by the one employed on the *xy*-plane ($P_\parallel$).

On the basis of previous reported works, in which negative pressures were applied to produce membrane rupture[67,68] or induced conformational variation of membrane proteins,[69] the lateral negative pressure to apply on the simulated membrane was calculated following the relation[70]

$$\gamma = \int_{-z}^{+z} (P_\perp - P_\parallel(z))\, dz \qquad \gamma = (P_\perp - P_\parallel) \cdot z_{thickness} \quad (8)$$

Where *γ* is the surface tension, and the integration is performed over the bilayer thickness. Knowing the surface tension of a double leaflet and its thickness, it is possible to calculate the lateral pression needed to impose a given stretching regime.

Brohawn et al.[21] suggested that an excised patch which contain a small fraction of the cell membrane (during a patch clamp experiment) should experience a patch pressurization because of the adhesion of the membrane lipids to the micropipette glass. The order of magnitude for a possible stretch activation due to the membrane adhesion ranged between 0.5-4 mN m^{-1}, although they also suggest an upper limit of 12 mN m^{-1} (membrane lytic tension). Nevertheless, there are examples of MD simulations of mechanosensitive proteins in the literature, where the stretching regime is imposed by higher pressures,[71] in order to overcome the time computing limitations. In fact, stretching activation occurs in the time scale of milliseconds. Since this time scale is currently out of reach for plain MD simulations, to speed up the sampling of membrane-induced conformational changes, higher tensions were intentionally used.[72]

The simulations were performed at the lateral pressure of -50 bar, corresponding to a surface tension of ≈ 25 mN m^{-1} (considering a bilayer thickness of 42 Å).

2.3 Simulations under physiological conditions: Ion concentration gradients and electrostatic potential

2.3.0 Ion concentration imbalance: state of the art

To overcome problems at the edges of the finite simulation cells, periodic boundary conditions (PBCs) are employed to simulate a large (literally infinite) system. The large systems approximated by PBCs consist of an infinite number of unit cells, where objects are allowed to cross through one side of the cell and to re-appear on the opposite side with the same velocity. On the one hand this feature allows to model bulk effects with a contained number of atoms. On the other hand, the periodic condition prevents from modelling separate solvent environments, which are indeed required to mimic in a reliable way membrane systems in physiologic conditions, where the ionic concentrations in the extracellular and intracellular sides are different.

In a pioneering study which dates back to 2003, Kalra and Hummer proposed a dual-membranes-dual-volumes strategy,[73] in which independent water compartments are separated by using two carbon leaflet nanotubes, to simulate osmotic translocations of waters molecules. The internal compartment, comprised between the two leaflets, was separated by the two externals, which were in contact through the upper and lower PBC of the unit cell. Kutzner et al. in 2011 exploited this setup controlling both ionic gradient and potential difference across the membrane, in order to simulate electrophysiological currents.[74] They embedded two porin channels within two membranes and mapped ions translocations through these.

Although the reported method presents useful features like the charges imbalance and potential difference directly regulated by the ion transport, it hides an unfavourable aspect: the size of the simulated cell becomes relevantly big, making it computationally demanding.

To allow the simulations of ion channels with a realistic implementation of asymmetric ion concentration, Khalili-Araghi proposed a straightforward method to control ions gradient across the unit cell.[75] The introduction of a nonperiodic “energy step” at the upper and

lower boundary of the simulation cell, is used to maintain and dynamically adjust a desired ionic concentration difference across the bulk phases.

2.3.1 The energy step: method and model

The "energy step" (ε) is literally a discrete force that act on all chosen particle that will be forced to remain in a specific bulk.

Let us consider a system consisting of a hydrophobic leaflet, which separates two bulk solutions of K^+ able to communicate through a pore (Figure 18).

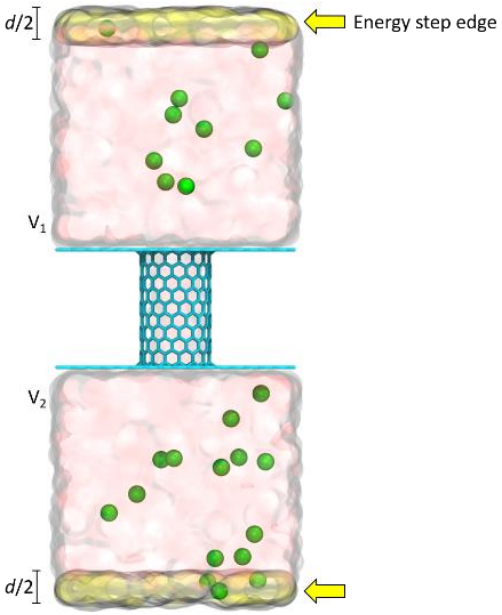

Figure 18. In figure is represented the model system consisting of a graphene slab separating two water bulks solution of K^+ ions. In yellow, in the bottom and top boundaries, the energy step is indicated.

If the system is described by a potential energy $U_0(\boldsymbol{\chi})$ which is a function of the atomic coordinates ($\boldsymbol{\chi}$), it can be said that the Boltzmann distribution is

$$\rho_0(\boldsymbol{\chi}) = \frac{e^{-\beta U_O(\chi)}}{\int d\boldsymbol{\chi} e^{-\beta U_0(\chi)}} \qquad (9)$$

where $\beta = 1/k_BT$. Focusing the attention only on selected species of the system, for example K^+ particles, at the light of the previous equation, the system can reach a uniform

concentration depending only by $U_0(\boldsymbol{\chi})$. For any configuration, the instantaneous number of K^+ in volume 1 (V_1 upper bulk) is

$$N_1(\boldsymbol{\chi}) = \sum_i \Theta(z_i) \tag{10}$$

where θ is a function of *z* coordinates, and is equal to 1 only when the particles are in the V_1. It is possible to enforce the condition that the average $N_1(\boldsymbol{\chi})$ will be equal to a chosen value $\bar{n}$ as such

$$\langle N1(\boldsymbol{\chi})\rangle = \int d\boldsymbol{\chi}\, N_1(\boldsymbol{\chi})\rho_0(\boldsymbol{\chi}) \tag{11}$$

where ρ_0 is the probability distribution. If there are *N* particles in the system, the condition should be such that $\bar{n} \leq N$. Ideally, it is possible to modify the statistical distribution applying a bias and modifying the probability distribution, imposing the condition that $\langle N1(\boldsymbol{\chi})\rangle = \bar{n}$.

Using the method of Lagrange multipliers, the probability distribution could be modified in a way such that

$$\rho(\boldsymbol{\chi}) = \frac{e^{-\beta[U_0(\chi) - k_B T\, \varepsilon\, N_1(\chi)]}}{\int d\boldsymbol{\chi}\, e^{-\beta[U_0(\chi) - k_B T\, \varepsilon\, N_1(\chi)]}} \tag{12}$$

where ε is an unknown coefficient that must be adjusted according to

$$\bar{n} = \int d\boldsymbol{\chi}\, N_1(\boldsymbol{\chi}) \cdot \rho(\boldsymbol{\chi}) \tag{13}$$

The form of $\rho(\boldsymbol{\chi})$ in eq. 12 is consistent with the introduction of a simple energy step, $k_B T\, \varepsilon \sum_i \Theta(z_i)$ that acts on all that particles crossing into the V_1 along the *z*-axis with a magnitude of $E = k_B T\, \varepsilon$.

Thus, it can be said that the average number of ions in the upper volume (V_1) can be approximated by assuming that the affected particles are nearly independent. The probability ($p = p_1 + p_2 = 1$) of finding the particles in V_1 (where $V_{tot} = V_1 + V_2$) can be written as a function of ε,

$$p_1 = \frac{V_1 e^{-\varepsilon}}{V_1 e^{-\varepsilon} + V_2} \tag{14}$$

as well as

$$p_2 = \frac{V_2}{V_1 e^{-\varepsilon} + V_2} \tag{15}$$

For a binomial distribution, the mean number of particles in V_1 is Np_1 and the variance is $Np_1(1-p_1)$: it follows that the average concentrations in the two bulks are functions of the probability to find them in V_1 or V_2 respectively

$$C_1 = \frac{Np_1}{V_1} \quad ; \quad V_1 = \frac{Np_1}{C_1} \tag{16}$$

that substituted in the eq.14, will result

$$C_1 = \frac{N e^{-\varepsilon}}{V_1 e^{-\varepsilon} + V_2} \tag{17}$$

and

$$C_2 = \frac{N}{V_1 e^{-\varepsilon} + V_2} \tag{18}$$

From the eqs. 17 and 18, it follows that ε is able to control the concentration ratio between two bulks in contact through PBCs

$$\frac{C_1}{C_2} = e^{-\varepsilon} \tag{19}$$

Assuming the two bulk volumes are identical, ($V_1 = V_2 = V_{tot}/2$) and substituting concentration C_1 and C_2 gives

$$C_1 = 2C \frac{e^{-\varepsilon}}{e^{-\varepsilon}+1} \qquad C_2 = 2C \frac{1}{e^{-\varepsilon}+1} \tag{20}$$

The range of the concentration ratio achievable is controlled solely by the energy step (in units of k_BT).

Considering that PBCs replicate the system also in the *z* direction (connecting the two aqueous bulks) a small transition region of thickness *d/2* is defined at the edges of the periodic box. Here an external constant force *f* directed along the *z*-axis acts on the specified ions. Thus the non-periodic energy step ε is defined as

$$\varepsilon = \beta \vec{f} d \tag{21}$$

where β is $1/k_BT$, *f* is the applied force and *d* is the edge thickness which alters the potential difference between the ions in the two bulks, generating a constant ratio of

$$r = \frac{C_1}{C_2} = e^{-\varepsilon} \quad (22)$$

The "energy step" strategy, was initially tested on a small model system, reminding the one proposed by Khalili-Araghi et al[75]. It was composed by two graphene leaflets separating two aqueous solutions of KCl and NaCl. In a rectangular simulation box of 40 x 10 x 100 Å containing the two "fictious" membrane leaflet, a graphene nanopore was embedded (sheet-tube-sheet system). The dimensions of this non-selective cylindrical channel were: radius 12 Å and length 20 Å. The simulations were performed using NAMD2.10 .The system was heated up to the temperature of 300 K and pressurized to 1 bar. To avoid volumetric fluctuations of the simulation box, the simulations were conducted in NVT ensemble. For the electrostatic interactions PME method was used with a grid spacing of 1.0 Å, whereas long range interactions were cut-of at 12 Å, with switching distance of 10 Å. All the hydrogens were restrained to the heavy atoms through the LINCS protocol. The simulations were run for 5 ns, with a time step of 1 fs. The "energy step" procedure was implemented in NAMD 2.10 through an in-house TCL script kindly provided by the developers.[75] The geometrical parameter "energy step" thickness (*d*) and the concentration ratio (*r*), were set to run the protocol, during a 5 ns long plain MD. In this context, the edge thickness was set to 10 Å, and a ratio (*r)* value of 100.

According to

$$\vec{f} = -\ln r \, \frac{k_B T}{d} \quad (23)$$

a negative force of 0.27 kcal mol^{-1} $Å^{-1}$ was imposed on K^+ ions, forcing them to reach the upper bulk. The sign of the applied force, comes with the concentration ratio in the presence of a logarithmic function, producing the imbalance showed in Figure 19-B,C.

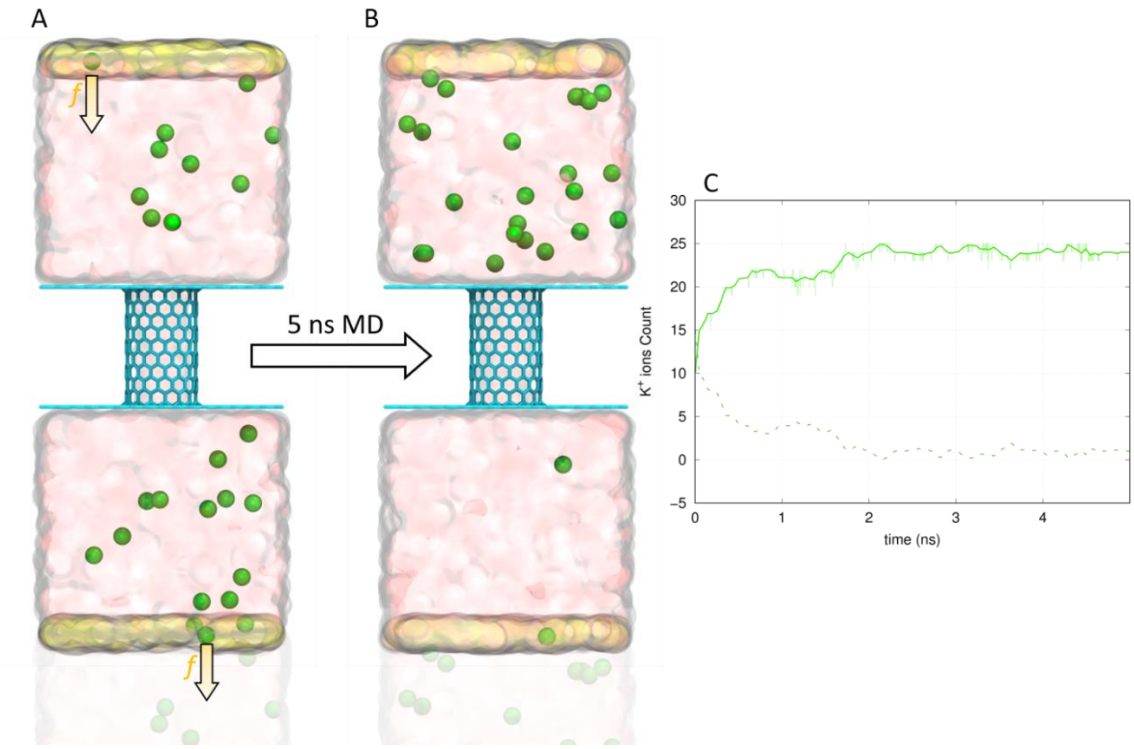

Figure 19. The energy step protocol applied along a 5 ns MD, produced a K^+ imbalance across the graphene slab. A) Is the starting configuration, where K^+ are nearly equally distributed in the two bulks; B) Is the final configuration, where the upper bulk was enriched in K^+ ions; C) is the evolutionary distribution of K^+ ions during the dynamics.

After 5 ns of plain MD in the presence of the "energy step" protocol, the K^+ imbalance was generated. The small force was selectively applied on K atoms, only when they cross the boundary of the unit cell, in a range of 5 Å per bulk. Stressing the separation process by using a high concentration ratio (r= 100), the convergence was reached after 2 ns, as is shown in Figure 19-C. When a K^+ of the lower bulk reach the bottom of the unit cell, f is switched on and the particle is forced to cross the boundary, flowing in the lower periodic cell, whereas when it reaches the top of the simulation cell it is forced to remain in the upper bulk.

2.3.2 The external field and electrostatic potential

To achieve physiological conditions by using MD simulations, and to allow ionic flow across channels, several approaches were proposed in the last decade.[76,77] Although the best adopted strategy consists in the imposition of an electrostatic external field (according to

the relation $\overrightarrow{E}$ = Φ/L), methodological ambiguities were evidenced by Gumbart et al.[78] The main argument addressed by the authors, comes from the length (L) on which the electrostatic potential should act. By choosing the length L value corresponding to the membrane thickness, an overestimated electric field is produced, so lower potential Φ is applied to the simulation box. In their work, Gumbart et al. demonstrated and proposed that the external field $\vec{E}$ should be directed perpendicularly to the membrane plane and might have a magnitude $\vec{E}$= Φ/L_z, where L_z is the length of the unit cell, instead of the double leaflet thickness. In the presence of a-priori known potential (for example the voltage applied during electrophysiological experiment) Φ and the magnitude of the related field depends only by the box size L_z.

By using this unconventional theory, it was showed that the electric field generates a linear Applied Potential across the entire cell, but the presence of a uniform medium (water) will naturally reorganize to reduce as much as possible the magnitude of any net average electric field.[78,79] The water medium is then redistributed in a non-uniform way which generates its own Reaction Potential that, when summed to the external, gives the Resulting total Potential Φ (Figure 20).

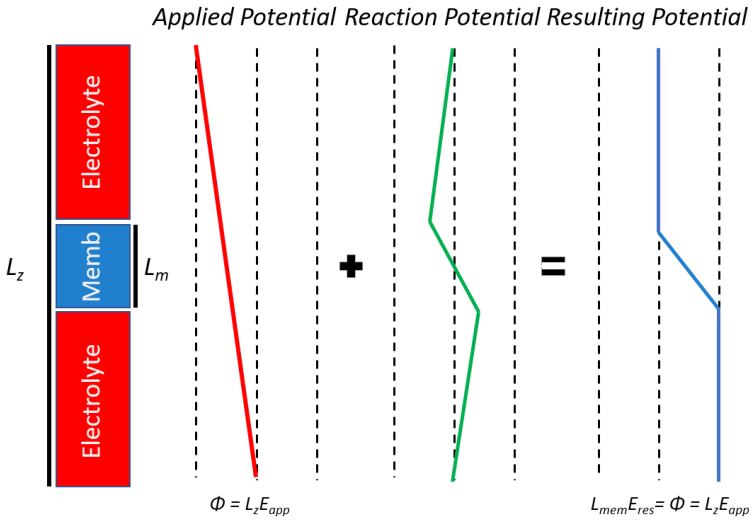

Figure 20. Schematic representation of the Resulting Potential (blue trace) acting on the simulated system, after the Electrostatic Potential (red trace) imposition, along the *z*-dimension of the unit cell. The Reaction Potential (green trace) is derived by the internal re-organization of the two bulk phases.

The resulting potential of the entire system matches the membrane region, despite a constant electric field is applied along the whole cell length. It can be said that the presence of the bulk phases, partially neutralize the Applied Potential confining it in the membrane slab proximity. The field represented in Figure 21, is effectively highly dense close to the carbon slabs, instead of in the bulk phase.

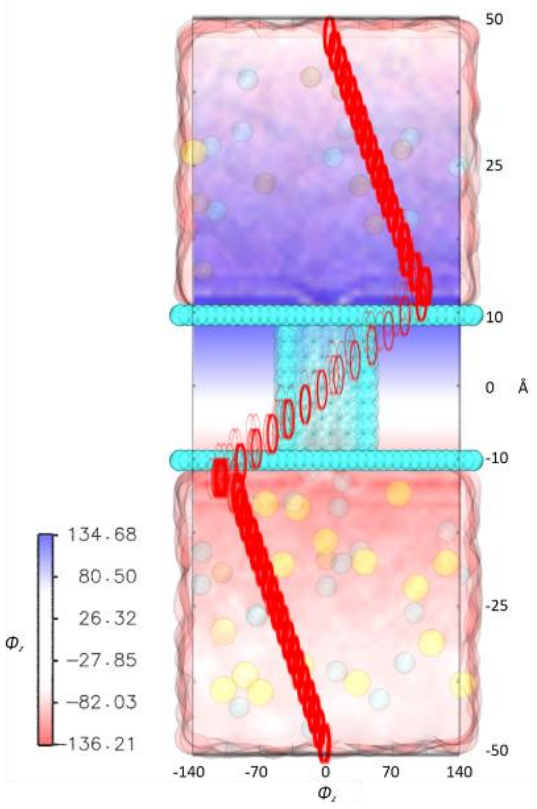

Figure 21. Representation of the simulated test case in presence of the electrostatic field. The blue and the red nuances in the bulk phases background represent the charges maps of the resulting potential. The red trace corresponds to *Φ(z) Vs* z *cell dimension.*

The electrostatic potential Φ was tested on the same test case used to explore the "energy step" method. The graphene sheet-tube-sheet system, separating an equimolar solution of KCl/NaCl, was inserted in a constant electrostatic field. $\vec{E}$ was expressed by the kcal mol^{-1} Å^{-1} e^{-1} units; one unit is equivalent to 0.0434 Volts/Å. Considering the relation

$$\phi = \vec{E} \cdot L_z \qquad (24)$$

and by choosing a target potential V and L_z value of 100 Å, results that

$$V = \vec{E} \cdot 100\ \text{Å} \cdot 0.0434 V/\text{Å} \quad (25)$$

The vector direction was chosen accordingly to produce a downward current of cations and, in light of the absence of selectivity by the nanopore, upward current for anions. The "energy step" was exclusively applied to Na^+ and K^+ ions in such a way to get cations depletion; upper bulk highly concentrated in K^+ and lower bulk in Na^+. The thickness *d* was set to 10 Å applied and the concentration ratio *r* to 100 for both cationic species.

In light of the system configuration, and in the presence of a negative potential across the pseudo membrane, an inward non-selective rectifying channel was emulated. The electrostatic potential operated such as an electromotive force (emf) applied to a physical circuit, generating ion flux through the nanopore.

A set of four simulations were performed varying the applied potential (2.5, 5, 10, 20 Volts), in order to test the system responses and measure K^+ currents. The 10 ns long performed simulations, were analysed by calculating the electrostatic potential as map of net charges, using the VMD tool PMEpot,[79]. The higher and lower values of charges were evidenced at coordinates *z*=-10 and *z*=10, equally distributed along the *xy*-plane. The effective potential difference experienced by the system, close to the dielectric slab, was given by the algebraic sum of the upper and lower potential values (in $k_BT\ e^{-1}$). Using T = 300 K, one unit of electrostatic potential is equivalent to 0.0258 Volts. The computed electrostatic potential (ranges from values reported in Figure 22, panel A) in $k_BT\ e^{-1}$ unit, were summed and converted in Volts. The resulting effective potentials were 1.9, 3.6, 7.0, 13.7 which were slightly close to the chosen initial target values.

The concentration gradients for K^+, Na^+, Cl^- (Figure 22, panel B, C, D) imposed by using of the "energy step" method were computed as volumetric maps (VMD VolMap tool) across the simulation box. The cations depletion was maintained for the entire simulations, resulting in a pseudo-physiological ion gradients for K^+ and Na^+; K^+ were mostly confined in the upper bulk, whereas the Na^+.in the lower. The presence of negative electrostatic field, by inducing downward K^+ flux, produced the enrichment of the lower bulk in potassium ions. The larger the potential applied, the bigger the transitory $[K^+]$ in the lower bulk, as is shown in Figure 22, panel B. The depletion of ions was restored by the presence of the

“energy step”. Na^+ were subjected to two opposite forces, resulting confined in the lower bulk. No currents were registered (no Na^+ ions densities were found inside the nanotube compared to the other two ions in the same simulation). Cl^- ions were subjected only to the forces produced by the electrostatic field, giving as final result outward currents. Cl^- ions were partially distributed between the two bulks, with a slightly higher concentration in the lower side, justified by the presence of the electrostatic field.

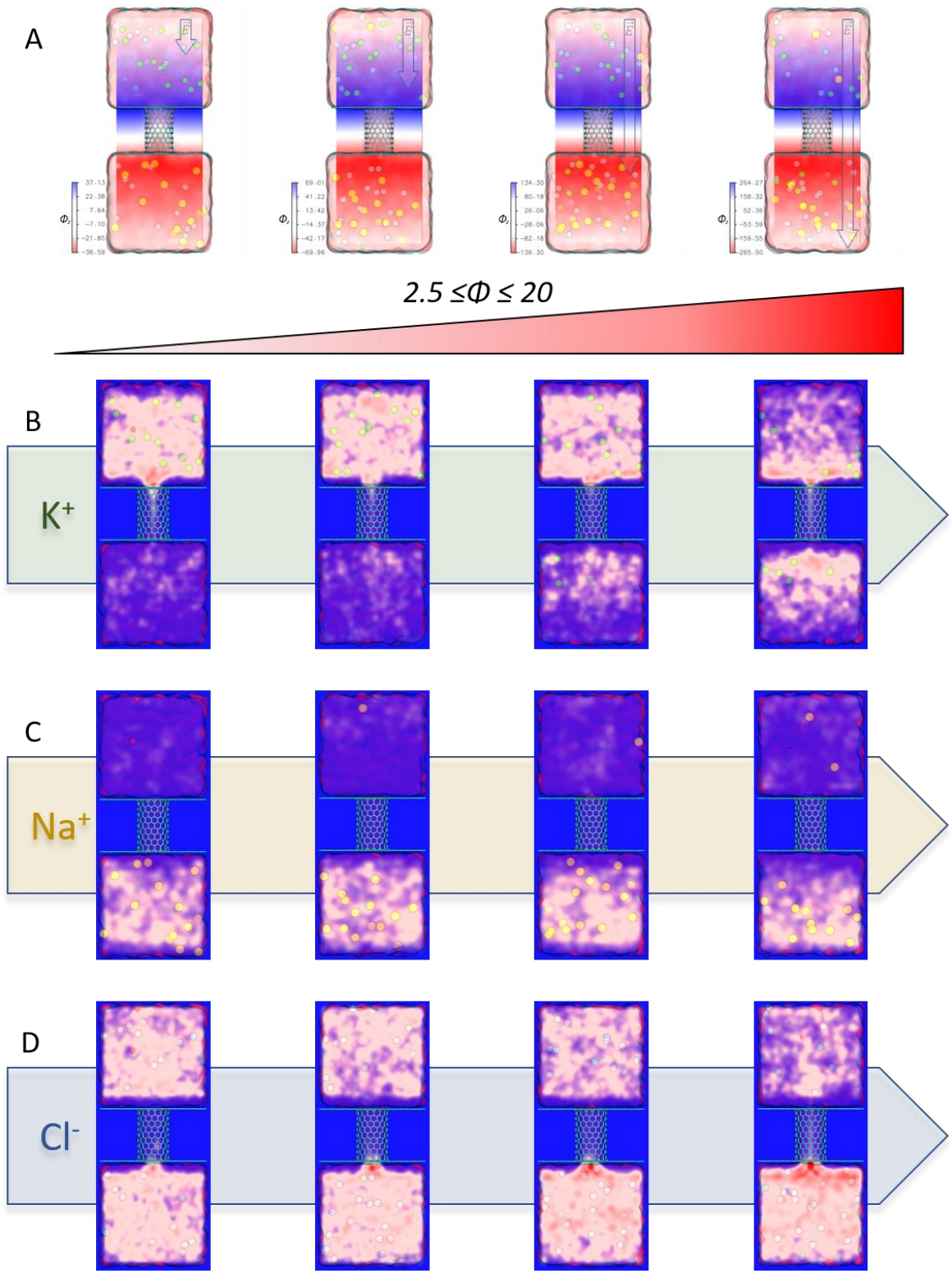

Figure 22. Schematic representation of simulated graphene sheet-tube-sheet in presence of increasing electrostatic potentials. A) Electrostatic PMEmap for all simulations; limit potential values are reported in according to the colour variation. B, C, D) Volumetric map of K^+ Na^+ Cl^- ions, in presence of increasing electrostatic potentials. In all figures green, yellow and cyan sphere represent K^+, Na^+, Cl^- respectively.

The final K^+ currents were calculated from the simulations and a linear relation was observed between the applied voltage and produced currents (Figure 23).

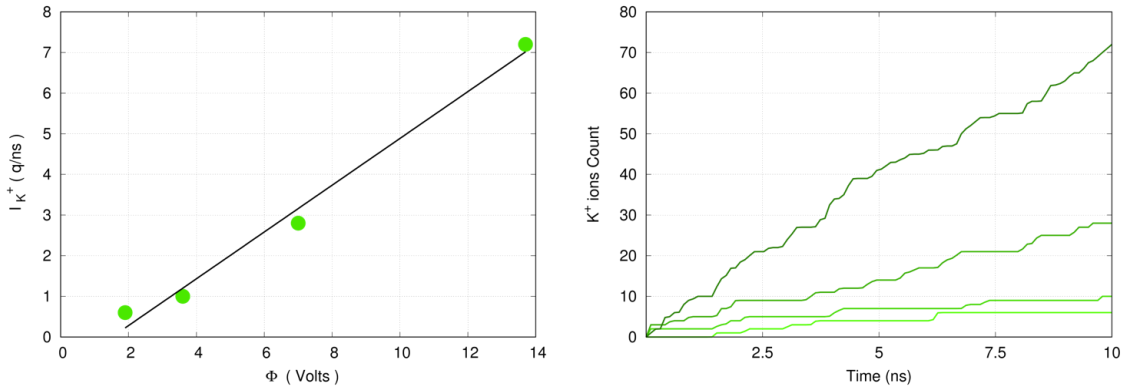

Figure 23. Time evolution of K^+ flux through graphene pore during 10 ns of MD simulation (A) and corresponding I-V curve (B**)**

2.3.3 hTRAAK in physiological conditions

The "energy step" method together with the electrostatic potential, applied to the sheet-tube-sheet system, were adapted accordingly to the hTRAAK membrane complex, to further investigate the channel behaviour in physiological condition.

In particular, the starting coordinates were taken from the ending structure obtained from **run-4i9w-b**; NAMD-2.10 MD software was used. The simulation setup was chosen to match as close as possible the one employed for plain MDs simulations, with the major differences being the thermostat algorithms. Langevin thermostat was used with a damping coefficient of 5 ps^{-1}, without the hydrogen coupling. The temperature was maintained at 300 K and all the simulations were performed in NVT ensemble. Electrostatic interactions were evaluated through PME, using a grid spacing of 1 Å. Short-range non-bonded interactions were treated with a cutoff of 12 Å, together with switching distance of 10 Å and the nearest neighbor search at 14 Å. PBCs were applied together with the "energy step". Specifically, considering eq.23, *d* parameter was set to 10 Å (sufficiently small to avoid any influence on particle far from the *z*-PBCs) and the concentration ratio *r* was set to 0.01 for both K^+ and Na^+. Considering the eq. 24 and the *z*-dimension of the simulation box of 150 Å, the electrostatic potential value Φ was set to +0.0155 Volts/Å, equivalent to an applied potential 100mV.

The simulation was performed without restraint to the protein heavy atoms. The restraints were selectively applied to the z-components of lipid's heads (phosphorous atoms), to prevent a shifting translation, characteristic during simulations in electrostatic potential. Concerning the K^+ configuration within the SF, coordinates were changed in order to get a partially hydrated one. Specifically, K^+ ions were located in S0, S2, S4, cage-like coordinating shells, whereas water was placed to S3 and S1. Firstly, 10 ns of equilibration to produce the ions depletion, was performed without the electrostatic potential, then the production was started. The simulations was carried out by using 2 fs timestep, for at least 500 ns.

3 Results & Discussion

3.1 Lipid occlusion investigation

3.1.1 Early insight of K^+ pathway obstructions from plain MD

Our investigations were started by using the putative non-conductive hTRAAK channel structure (PDB-code 4I9W). As was previously introduced, in the non-conductive crystal the two inner helices TM4 were found to adopt an asymmetric conformation. The TM4 of second subunit results to be slightly distant (less than 10 Å) from the opposite inner helix TM2A, leading to a fenestration opening in between (Figure 24-A).

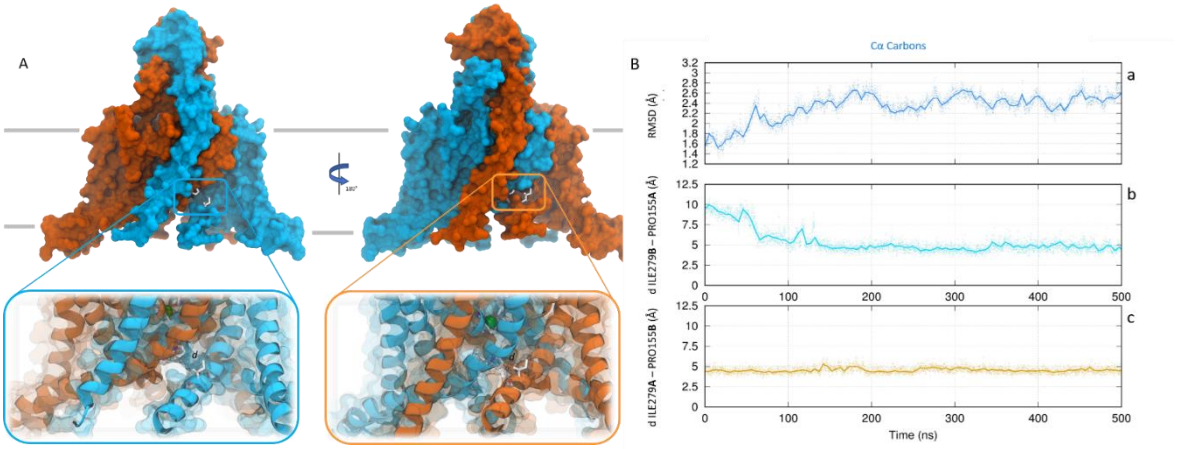

Figure 24. Pictorial view of side fenestration opening at TM4B/TM2A helices interfaces. Ba) The root mean square deviation (RMSD) of the simulated system along 500 ns. Bb,c) Distances distributions between key residues PRO155B-ILE279A

Conversely, the two inner helices of the opposite domain (TM4A – TM2B interface), were found to be in contact, preventing the side window opening. The asymmetric protein in complex with the membrane double leaflet, solvated in a symmetrical concentration of KCl, was simulated for 500 ns. Observing at the protein dynamical behaviour and by measuring the root mean square deviation (RMSD, Figure 24-Ba) of Cα atoms, the protein seemed to reach the stability at about 150 ns. We observed that the higher contribution to the RMSD fluctuations, came from the TM4B movement towards the up conformation, which is reached after 150 ns. The TM4B motion, was properly monitored by measuring ILE279-

PRO155 distance, which decreased down to ≈5 Å, assuming a symmetrical shape compared to the opposite subunit. Although the side fenestration seemed to be closed, by visual inspection of surrounding membrane lipids a distinctive behaviour was nevertheless observed. Since the beginning, one POPC molecule was found to enter the protein gorge from the lateral hole, reaching the cavity with the latest carbon atoms of the oleic-acid tail (Figure 25-Ab).

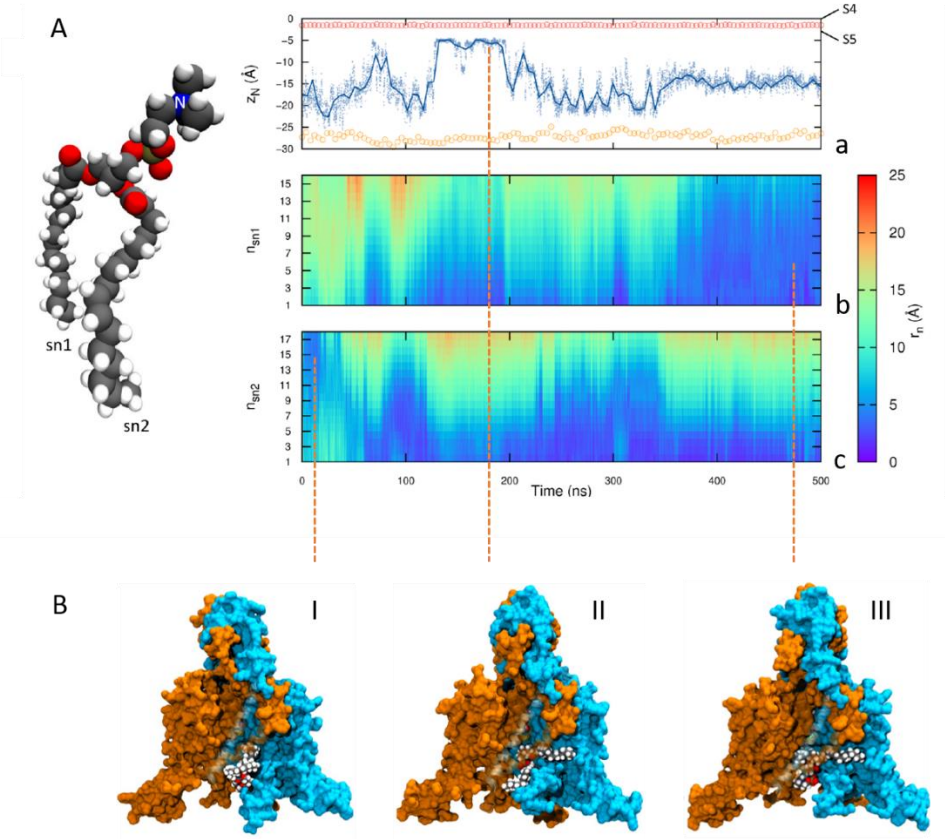

Figure 25. Distances distributions of hampering lipid within the hTRAAK gorge. Aa) plot of the distance between an hampering lipid polar head and the first coordinating shell. Ab,c) are the radial distances from the cavity, specifically from the ion pathway. BI,II,III are the three configuration found along the classical MD.

This initial "tail-dangling"(Figure 26-BI) configuration was maintained for at least for 50 ns, where the hydrophobic tail occluded the SF entrance. The obstructing lipid, after a transient of 100 ns, started to engage an interaction between the positively charged choline moiety and the threonine sidechain oxygens (the S5 coordinating lower plane, Figure 26-Aa). This "head occluded" (Figure26-BII) configuration was maintained for ≈ 70 ns, after which the lipid (entirely inside the cavity) flipped back, occupying the internal protein

volume with the palmitoyl sidechain. Here the aliphatic tail was completely curled up close to the SF entrance. We called this third obstructing conformation “tail occluded” (Figure 26-Ac, 26-BIII). By looking at all three configurations, the obstruction occurred within a distance of less than 5 Å from the SF, making the Brohawn hypothesis of lipid blocking arguable as it stands.[21] This simulation, revealed the potential lipid existence inside the cavity and seemed to preclude the K^+ ions access to the SF. To test these circumstances, starting from those three structures, further investigations of K^+ translocations from the inner cavity up to the SF were carried out.

3.1.2 The lipid hampering of K^+ flow

The three representative configurations mentioned above, were extracted from the 500 ns long **run-4i9w-lip** and used as starting conditions for three independent WTmetaD simulations. In particular we chose to investigate the lipid hampering produced by the three alternative obstructive moieties. The POPC molecule was thus confined inside the inner cavity, applying a cylindrical shaped upper wall restraint (KAPPA=4184 $kJmol^{-1}nm^{-2}$), in order to preserve its conformation. The CVs selected as reaction coordinates to explore the lipid ability to block the ionic flow, has been: the projection of the z cartesian coordinate of a K^+ ion along the channel axis, and the radial distance from that axis. In this way, we were able to describe the ionic flow of an approaching K^+ ion to the first coordinating shell of the SF (S5 threonine oxygens plane, Figure 26).

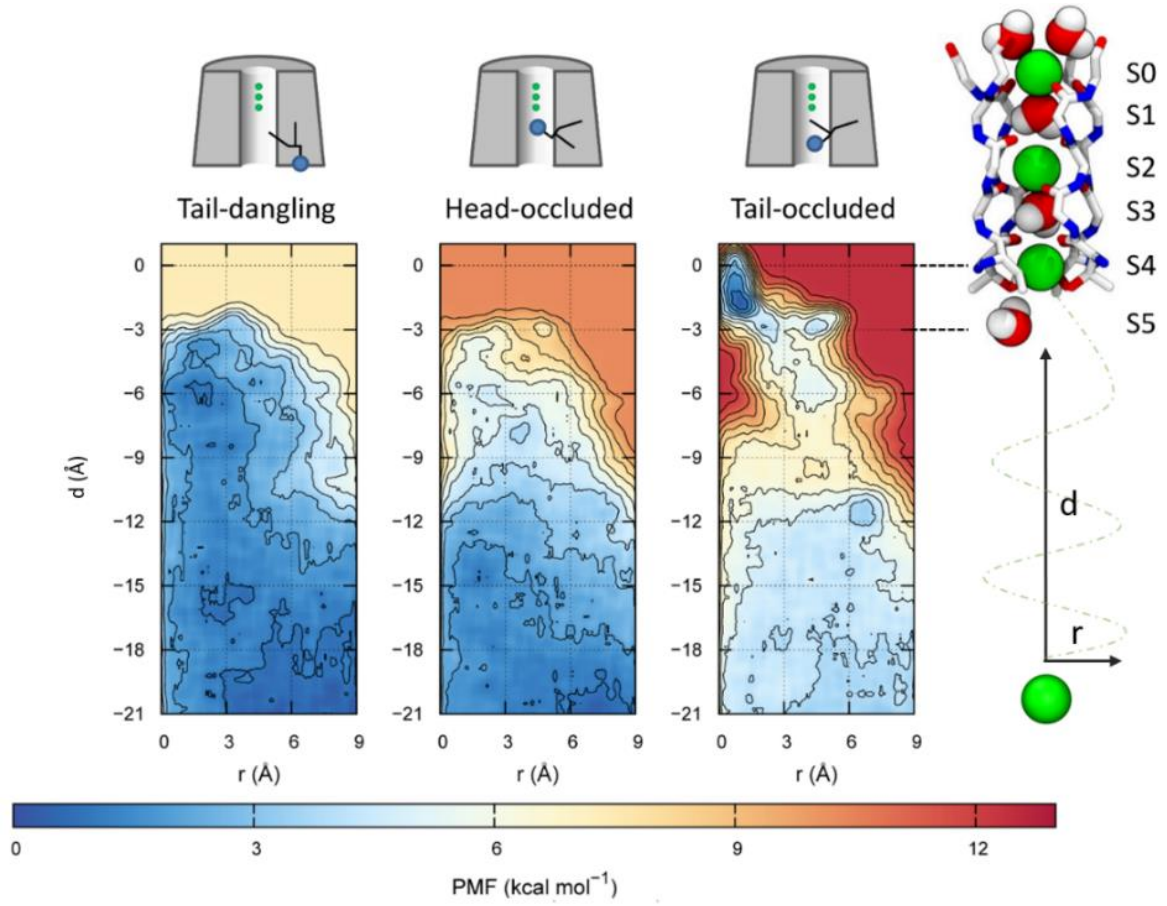

Figure 26. Poteintial of Mean force profiles of K^+ ions twords the SF. In the trhee panels are represented the free energiy surfaces of related lipid hampering configurations. In the right pictures, are presented the two CV used to as reaction coordinate to quantify the lipid hiderence

What we expected to find, was a flat energy profile far from the SF (corresponding to the free diffusion of the solvated ion in the bulk water cavity), and increased energies approaching the SF, because of the presence of steric hindrance played by the lipid. Actually, this hypothesis was consistent with the potential of mean force (PMF) gained by the WTmetaD in two cases out of three. When the lipid adopted the "tail dangling" conformation, the steric occlusion provided by the oleic- tail, was not sufficient to impede the K^+ translocation to the S5 site (Figure 27). The FES obtained from the first simulation, resulted to be flat until the initial weak coordination performed by the threonine oxygens sidechains ($d \approx 3$ Å). The presence of the aliphatic tail did not prevent the potassium access to the channel pathway, and so a flat profile with a barrier lower than 2 kcal mol^{-1} was found.

Slightly different results came from the WTmetaD performed starting from the "head occluded" configuration. Essentially, due to the charge-dipole interaction engaged by the positive nitrogen choline head, a substantial occlusion take place. A sizable barrier to the order of ≈ 5 kcal mol^{-1} was obtained. It is worth noting that in the S5 site, threonine oxygens were seen to be involved in a competitive coordination between the POPC hydrophilic moiety and the K^+ ion, which was forced to remove the charged head to be coordinated.

Finally, in the last configuration the picture did not dramatically change. From the "tail occluded" state, a significant decreasing of cavity volume was observed mainly due to the curled up conformation adopted by the oleic- tail. A transition state of ≈ 4 kcal mol^{-1} was found 6 Å far from the S5 site, in the same region of the occluding acyl chain. Notably, the S4 site, i.e. the first internal coordination site of the SF from the intracellular side of the membrane, was also sampled.

To understand how relevant were these free energie differences for the initial translocation process, we compared them with previously reported results.[80,81] It is well-known that, to achieve a high rate of conduction, K^+ channels require an ion permeation pathways with barriers of no more than 2-3 kcal mol^{-1}. Thus, the reported results were found in good agreement with an efficient flow of K^+ ions through the considered "tail dangling" state but not for the occluded states. Our findings are also in partial agreement with the Brohawn hypothesis of lipid occlusion by considering the spontaneous insertion of a POPC molecule in the protein cavity when it is in the up/down state, but it still remains unclear if the lipid hampering is actively involved in hTRAAK gating mechanism.

3.2 Membrane stretching investigations

3.2.1 General overview of protein behaviour in conventional MD

The results showed above, gave preliminary insight about the direct implication of individual lipids in the conduction process through hTRAAK channel. However, at this stage, no more hypothesis could be done about the membrane induced gating mechanism. In this context, the role of membrane deformation in the spontaneous lipid insertion process

and/or in the transition between the conductive/non-conductive states remains to be clarified.

In this part of the study, we attempted to provide a comprehensive framework of the protein behaviour by simulating the hTRAAK in the NPT ensemble at room temperature/pressure, as well as by applying negative pressure, with the aim to produce a controlled membrane stretching.

Being aware of the spontaneous transition from an up/down to the up/up conformation observed during the **run-4I9W-lip** (see Figure 25-B), we decided to start a new set of simulations by using all four crystals stored in the Protein Data Bank, representative for both states. In details, 4WFE and 4WFG crystal structures were found in the archetypal conductive state where both TM4s adopts an “up” symmetric conformation; 4I9W and 4WFF crystals representative for the non-conductive state, in which the TM4B in “down” conformation leads to the side fenestration opening. Three simulations were run for each embedded channel, consisting of twelve independent runs (see chapter 2.2). We have chosen to perform triplicate simulations per crystal structure considering the following reasoning. First, we wanted increase the statistical sampling for each starting conformation in order to understand if the lipid insertion was only a spurious/random event. Second, by starting from two putative opposite states, we extended the conformational space to explore. These twelve runs were used to determine the main protein fluctuations along 200 ns of dynamics (aggregate time: 2.4 μs). Indeed, the root mean square fluctuations (RMSF) of all Cα atoms were calculated, to identify the main stability regions of all complexes (Figure 28-Aa-d). It was not surprising that the SF domain resulted the region with higher stability, such that the residues fluctuations were found below a threshold value of 0.5 Å. Conversely, the highest flexibility was shown by the helical cap and the external loops (2.5 Å ≤ RMSFs ≤ 4.5 Å). Finally, concerning the TM helices, residues showing high motility were mainly found towards the intracellular side than the extracellular.

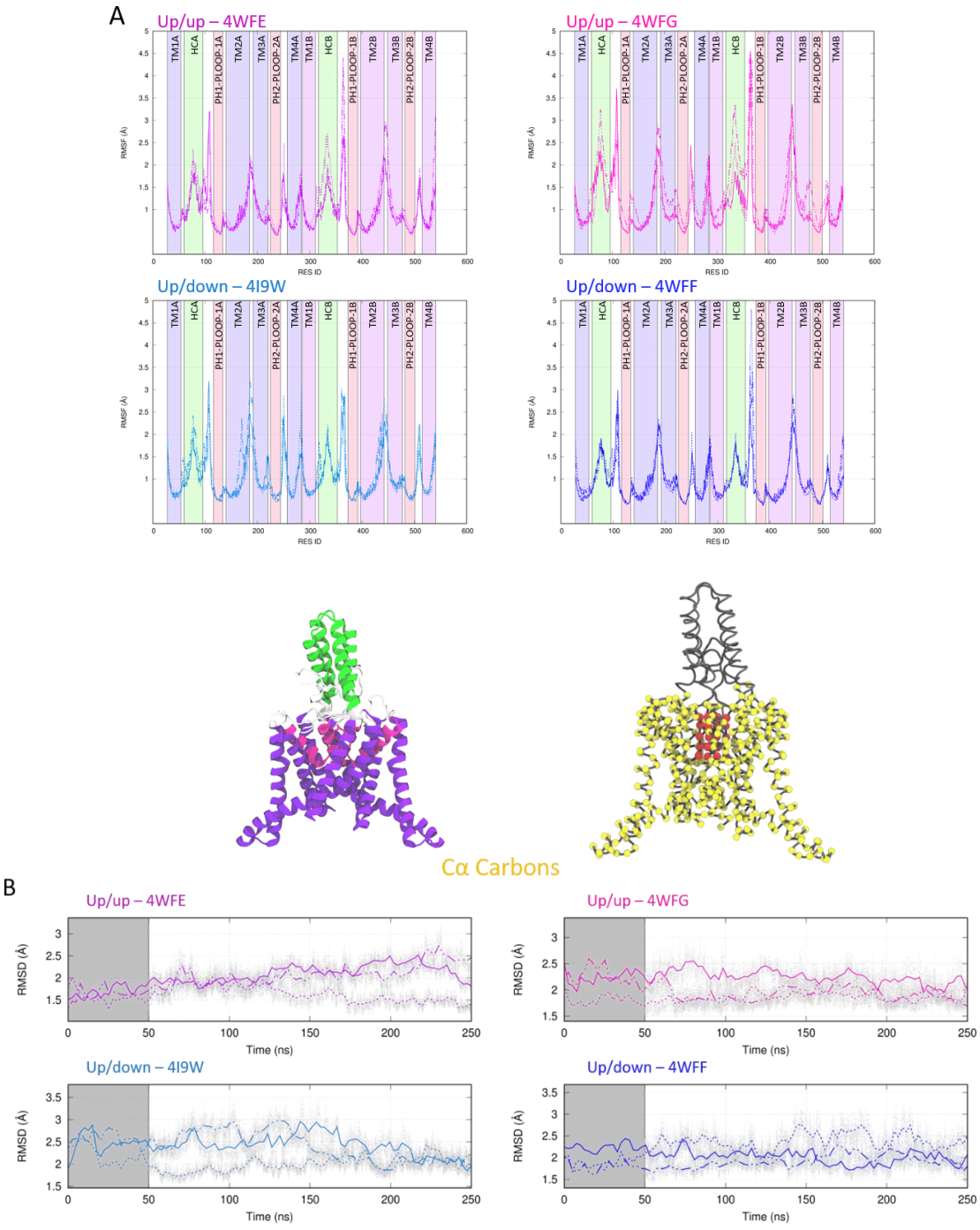

Figure 27. RMSF and RMSD Analysis. A) RMSF profiles calculated by all Cα atoms, grouped according to the starting hTRAAK conformer. The background panels, are coloured according to the protein segments. B) RMSD profiles calculated by using all TMs Cα atoms. Bold, dashed and dotted lines are referred to run-4wfe,4wfg,4i9w,4wff-a,b,c respectively

In line with the expectations, large fluctuations of the TM4B were observed. Essentially, in **run-4i9w-a, b, c** and **run-4wff-b,c** fluctuations were found up to 2 Å, whereas for the remaining, the larger ones were of 1.5 Å. Like in the **run-4i9w-lip**, a fast rearrangement of the TM4B to an "up" conformation, was achieved. Finally, concerning the TM2s and TM3s helices, the ending and starting residues, respectively, were found to give the main contribute to the RMSF, which showed higher fluctuations up to 2.5 Å.

Considering the high stability showed by SF residues, Cα carbons were selected for the protein alignment, whereas the residues of the helical cap and external loops (with highest motility) were excluded from the selection used to calculate the root mean square deviation (RMSD, Figure 28-Ba-d). The crystal structures were used as reference. Once more, the initial 50 ns which were considered as equilibration were excluded from this analysis, and only 200 ns for each simulation were used to evaluate the protein stability. The RMSD values reported in Figure 28-B, shows the overall stability of each conformer, with peaks always lesser than 3 Å.

3.2.2 hTRAAK essential motions

From the results gained by the RMSF and RMSD analysis, it was not possible to observe a substantially distinct behaviour of the TM4s among the simulations; neither comparing each replica of a specific conformer, nor from different groups of conformers. Thus, to overcome this issue, and in the attempt to identify potentially related conformational movements, a principal component analysis (PCA) was carried out. Taking into account that the putative region involved in the channel activation might be the TM2/TM3/TM4 interfacial domain, we chose to extract the eigenvectors associated to the TM4s helices main motions. In particular, all trajectories were concatenated in a 2.4 μs long trajectory and analysed. Cα carbons of the SF were used as alignment selection, and the measurement was performed using all atoms belonging to the TM4s (from proline 255 to the C-terminus). To get an idea of the explored conformational space, we plotted the projections of the first two eigenvectors. The eigenvalues associated to those two eigenvectors, were considered sufficiently large, to be representative of the main motions of TM4s domains. The

percentage contribution of the first eigenvector covered the 30% and the second 15% of the total motion.

The first principal component (Figure 28), describe such opening movement of both helices towards the membrane along the *xy*-plane. It shows a large variance, ranging between values -4 and 8.

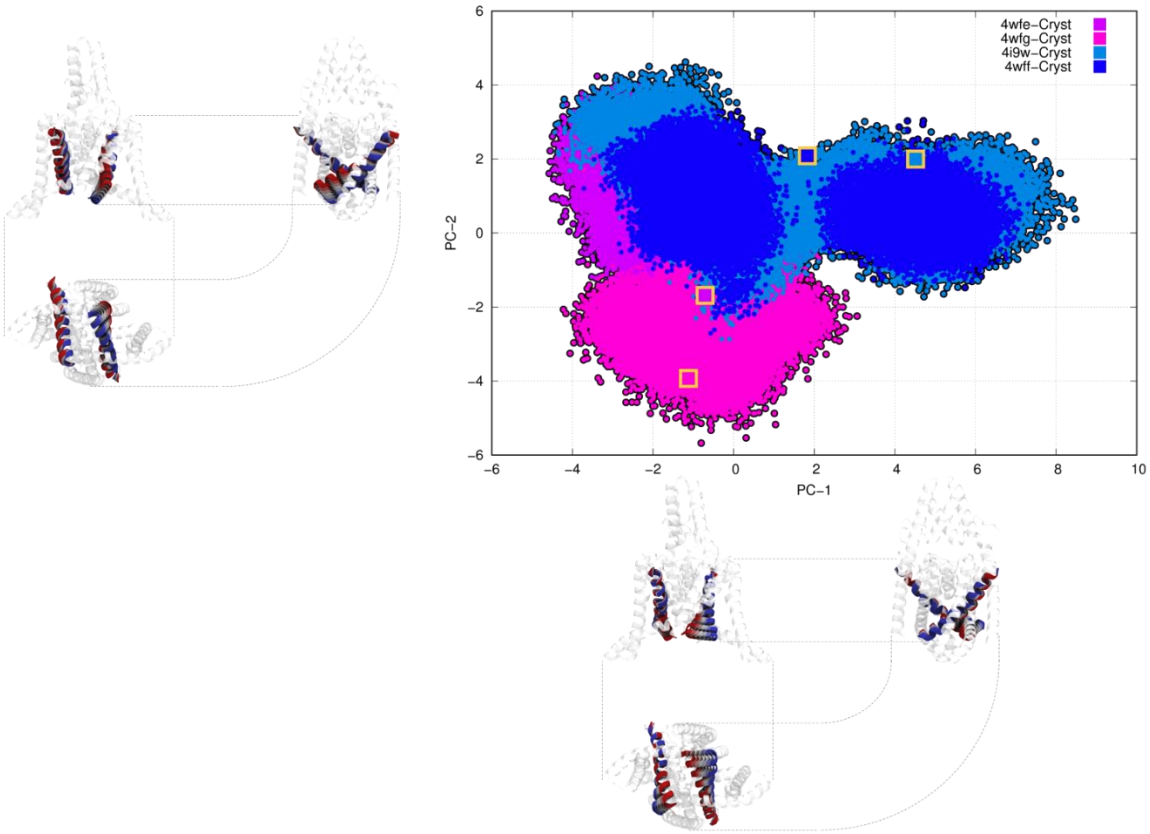

Figure 28. Principal component analysis of Transmembrane helices 4. The first vector (PC-1) describe the cavity expansion. The second eigenvector (PC-2) describe the "up to down" transition of TM4B.

Focusing on PC-1, and observing the motion looking at the channel from the bottom and side views, TM4B range over a larger space compared to the opposite helix, in line with the expectation considering its starting conformation. The main contribution to the second principal component (PC-2), apparently comes from the TM4B helix. PC-2 describes the "up to down" movement of the TM4B, whereas the TM4B shows only small fluctuations. Even though two main eigenvectors seem to describe the same motion, they are useful to identify at least two different regions in the conformational space. The largest amount of

frames of the whole trajectory was found in the left side of the plot , whereas a smaller number of frames were found to be located in the right side. Decomposing the graph, and plotting the single conformers contribution on the same space (Figure 29-A,B), a good overlap between **run-4i9w-b** and **run-4WFF-c** in regions distant from the remaining frames was observed.

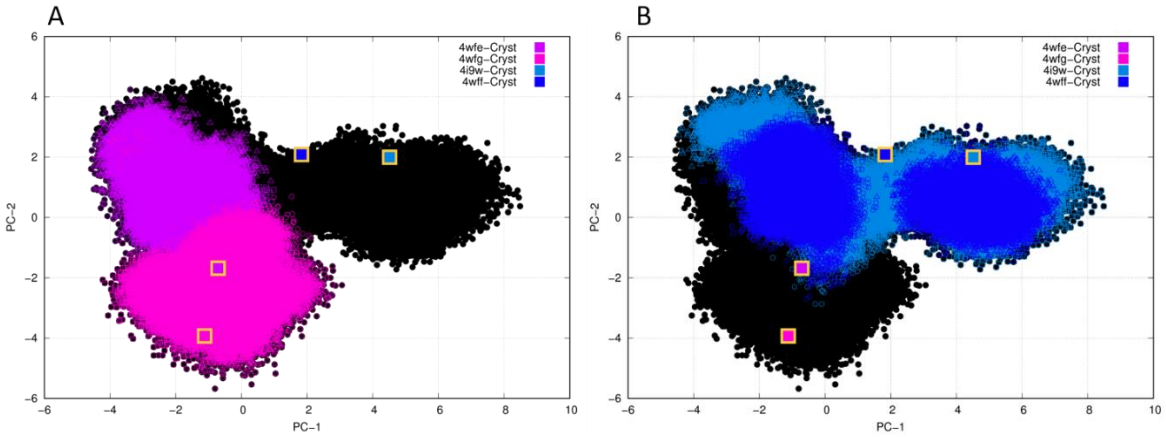

Figure 29: Decomposed PCA analysis. A) Frames projections of up/up runs "run-4wfe-a,b,c" (purple) and "run-4wfg-a,b,c" (magenta) on the principal components vectoral space; B) projections of up/up runs "run-4i9w-a,b,c" (light blue) and "run-4wff-a,b,c" (dark blue). Runs a,b,c are represented in coloured dots ○, □ ,△ respectively

Moreover, considering the projection of the four starting crystals, it becomes clear that the protein along the simulations try to converge towards the up-left region of the PC space, corresponding to an "up" conformation of the TM4B (larger values of PC-2) and expanded along the membrane plane (lower values of PC-1).

In conclusion, the PCA turned out to be instrumental to identify the relevant conformational motion associated to TM4s helices.

By measuring the distances between the key residues ILE275-PRO155 already used during the lipid-blocking experiments (see chapter 3.1.1), it was possible to further investigate the TM4B motion. During the entire simulation and in every complex (except the above mentioned two runs and for **run-4wfe-c**), distances between TM2s and TM4s were found in a range comprised between 4.5 and 7.5 Å, in line with the results obtained from **run-4i9w-lip.** The side hole at TM2/TM4 interfaces resulted to be closed and not occluded by any lipid except for those three cases; in fact distances over 7.5 up to 10 Å were measured (Figure 31-A,B)

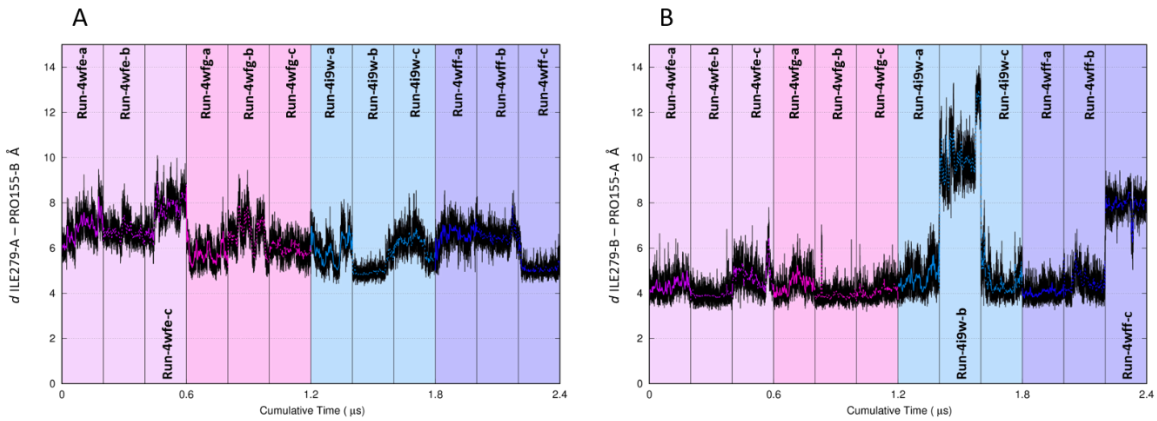

Figure 30. Distance measured between TM4 and TM2 helices plotted against the aggregate time of the twelve simulations. A) TM4A-TM2B distance. B) TM4B-TM2A distance. Bold, dashed and dotted lines are referred to run-4wfe,4wfg,4i9w,4wff-a,b,c respectively.

3.2.3 Classical MD under membrane stretching conditions

With the analysis performed so far, we attempted to provide a comprehensive picture to describe the protein motion regarding those domains involved in the putative activation mechanism. In order to gather relevant insight related to whether and how the protein could exploit the membrane deformation, a further ensemble of MD simulations were performed, applying a constant pressure of -50 bar (corresponding to ≈25 mN m^{-1}) on the *xy*-plane of the unit cell.

The simulations were started from the 100th ns of the twelve runs performed in NPT ensemble. The simulations were carried out for further 200 ns. This choice was particularly useful because it allowed us to investigate what was the direct influence of membrane stretching on the cavity surroundings lipids eventually involved in the blockage process.

The RMSD (Cα atoms of SF domain used for the alignment and protein transmembrane Cα for the measurement, Figure 32-A-D) showed larger fluctuations with respect to plain MD simulations. In eight cases over twelve, RMSD were found significantly increased up to 4.5 Å. Moreover, in none of the investigated simulations a stable conformation could be reached.

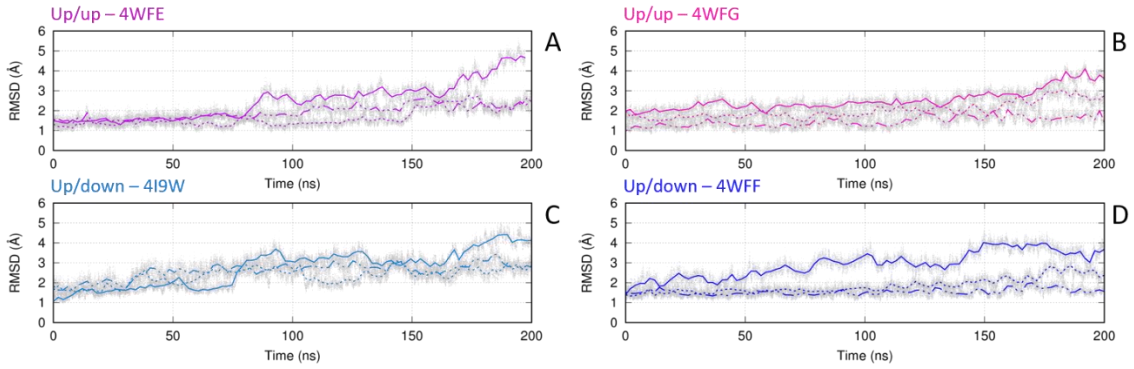

Figure 31. RMSD profiles calculated from the simulations under membrane stretching conditions. Bold, dashed and dotted lines are referred to run-4wfeST,4wfgST,4i9wST,4wffST-a,b,c respectively

Again, the distances between the above mentioned key residues (PRO155-ILE279 monitored during the NPT simulations) were informative to understand if the interfacial domain underwent relevant changes, namely if the side fenestration opening was affected by the membrane stretch. By looking at the distances (Figure 33-A,B), immediately appeared evident the influence of the stretching on TM4s displacement from the original positions.

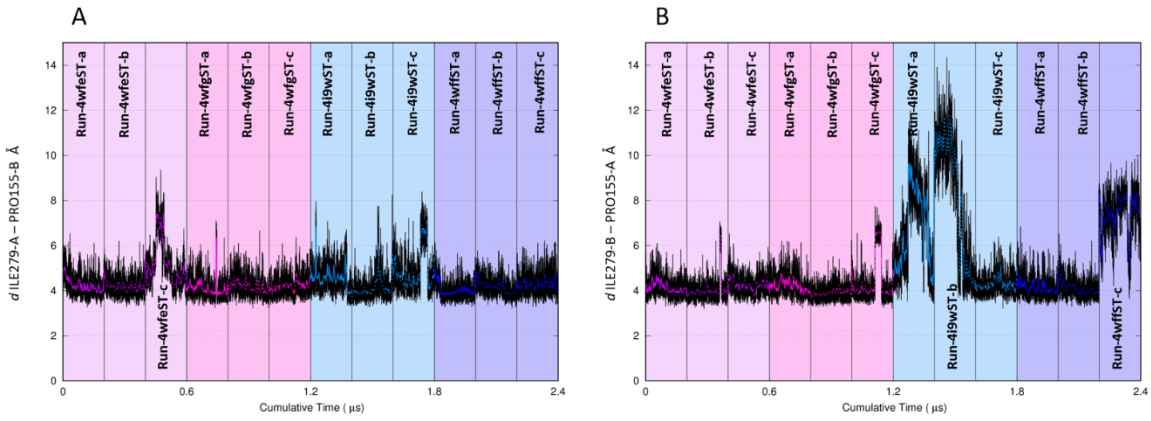

Figure 32. Distance measured between PRO155 and ILE279 plotted against the aggregate simulation time. A) TM4A-TM2B distance. B) TM4B-TM2A distance. Bold, dashed and dotted lines are referred to run-4wfe,4wfg,4i9w,4wff-a,b,c respectively. Graphs background is coloured according to the reference crystal structure

After the first 100 ns in which the protein maintained the same conformation of the previous corresponding simulation, the distance between the two helices was rapidly reduced from 10 to 5 Å in **run-4i9w b**. Observing **run-4i9w-c**, several spikes were found in

the plot. In this case, the protein was trying to reduce the interhelical separation, but a stuck lipid prevented this conformational change to fully take place.

In general, a significant reduction of the interfacial separation was observed in all runs. Thus, we can conclude that membrane stretching seems to play a role in the conformational transition of the protein which can be in turn related the opening/closure of the side fenestration.

The results showed so far, have depicted a conformational transition from down to up of the asymmetric TM4B, induced by membrane stretching. An in-depth analysis of individual trajectories revealed another important conformational change with potential implications on the gating mechanism, that is the cavity expansion. The measurement of distances between the two opposite ILE279 (namely TM4A-TM4B distance, Figure 34-A-C) at membrane equilibrium and under membrane stretching showed an evident distinct trend. Interestingly, except for **run-4wfg-b** and **run-4i9w-a**, in all cases the distances between the TM4s tended to be reduced, and so the volume of the protein gorge was reduced as well. But when the negative pressure started to stretch the membrane, the protein reacted expanding its cavity (see Figure 34-B,C).

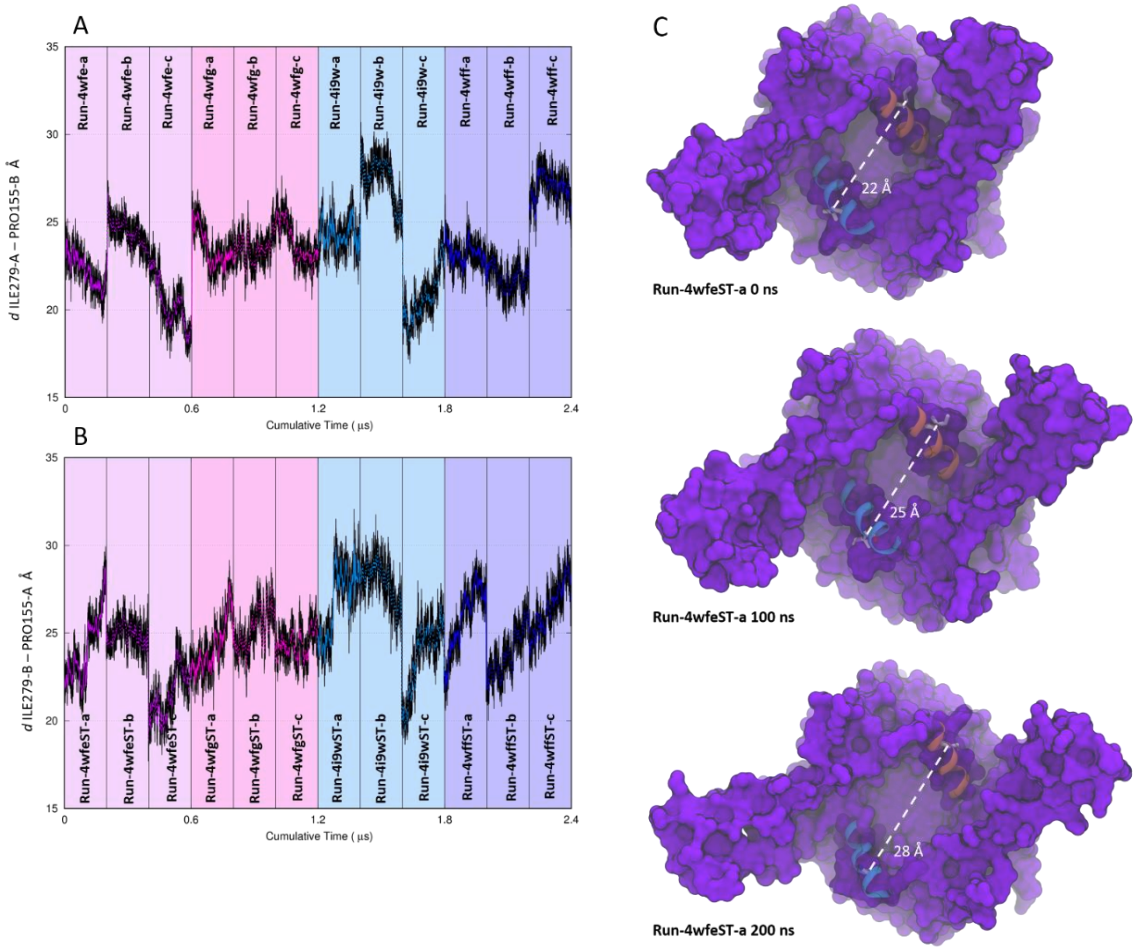

Figure 33. Distances measured between ILE279 of TM4A and TM4B. A) distances measured at membrane equilibrium B) distances measured at negative pressures. Bold, dashed and dotted lines are referred to run-4wfe,4wfg,4i9w,4wff-a,b,c respectively. Graphs background is coloured according to the reference crystal structure. C) pictorial representations of three key conformations adopted by hTRAAK during the run-4wfeST-a. Distance between ILE279A and B (white dashed line) is indicated.

The extent of hydration was also analysed by counting the number of water molecules located in the cavity, and the number K^+ ions able to reach to the SF. The analysis was performed on both equilibrium and membrane stretching simulations. In Figure 35-A,B, two limiting cases are reported: on one side, we observe large hydration of the protein gorge during **run-4wfeST-a**, larger if compared to the equivalent property measured in **run-4wfe-a**. Conversely, in **run-4i9w-ST-b** although the closure of the side fenestration was observed during the run, the water volume inside the cavity was reduced as well as the distance between TM4A-TM4B (compare Figure 33-A, Figure 33-B and Figure 34-B).

During the simulation under membrane stretching, the number of water molecules was increased up to 90, whereas at membrane equilibrium, it slowly decreased down to 55. In

the case of **run-4i9w-b** and **run-4i9wST-b**, the volume remained approximatively the same (≈ 75 molecules), although it was still bigger than the previous case. As a consequence, at high hydration, a correspondingly increased number of ions is able to flow from the intracellular water bulk to the cavity.

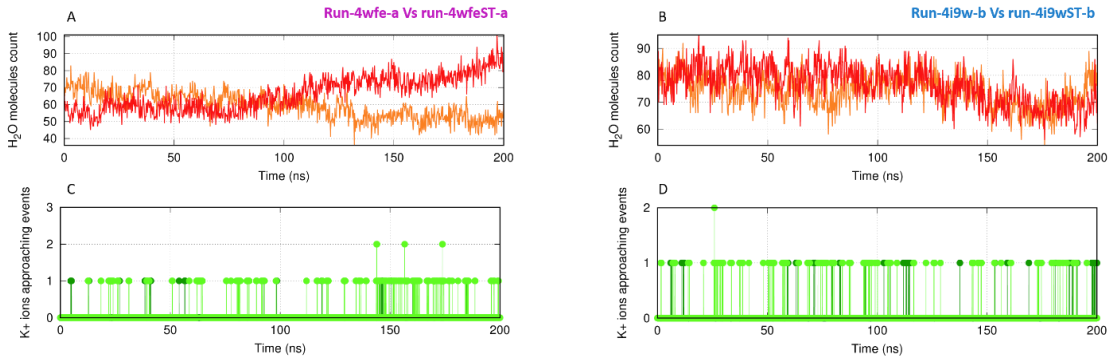

Figure 34. Time distribution of water molecules (upper panels) and K^+ residence in the within the hydrated cavity, measured from the related simulations in membrane equilibrium (orange traces, dark green spots) and membrane stretching (red traces, light green spots)

3.2.4 Membrane stretching promotes the lipids removal

Another interesting evidence concerning the proximal lipids displacement from the channel cavity, came out from the simulations under membrane stretching. Relevant information about the potential lipid occlusion were previously elucidated (chapter 3.1), but this new set of simulations suggested a direct involvement of lipids in the protein conformational changes.

Considering those two runs (**-4i9w-b, -4wff-c**) in which TM4B is in down conformation (TM4B-TM2A distances up to 10 and 8 Å respectively, Figure 31-B), by visual inspection, at least one lipid into the side window at the TM2A/TM4B interface was found. In one case (**run-4i9w-b**) the lipid was found to get stuck inside with the oleic- tail (in analogy to the previously discussed "tail dangling" configuration, chapter 3.1), whereas in the second one (**run-4wff-c**) it was found to reach the protein cavity with the choline moiety (in analogy to the previously discussed "head occluded" conformation, see chapter 3.1).

The presence of a stacked POPC molecule (Figure 36-Ba-c, 37-Ba-c), should reasonably justify the stability of the "down" conformation, found in those two runs, in which TM4B was maintained significantly separated from TM2A. Potentially, the shorter time scales of

those two simulations (if compared with the 500 ns long **run-4i9w-lip**) was not sufficient to perfectly match the previously identified configuration: the hampering in the two considered run was in an early stage. However, by stretching the membrane at negative pressure condition another important event (concomitant with those showed above, namely the side window closure and the cavity expansion) was noted: surrounding lipids, were slowly pushed out from the cavity (Figure 35) The starting configuration of **run-4i9wST-b** and **run-4wffST-c**, had a POPC moiety inside the protein gorge. During the 200 ns of stretching, those lipids were forced to follow the membrane motions, increasing their distances from the ion pathway within the cavity.

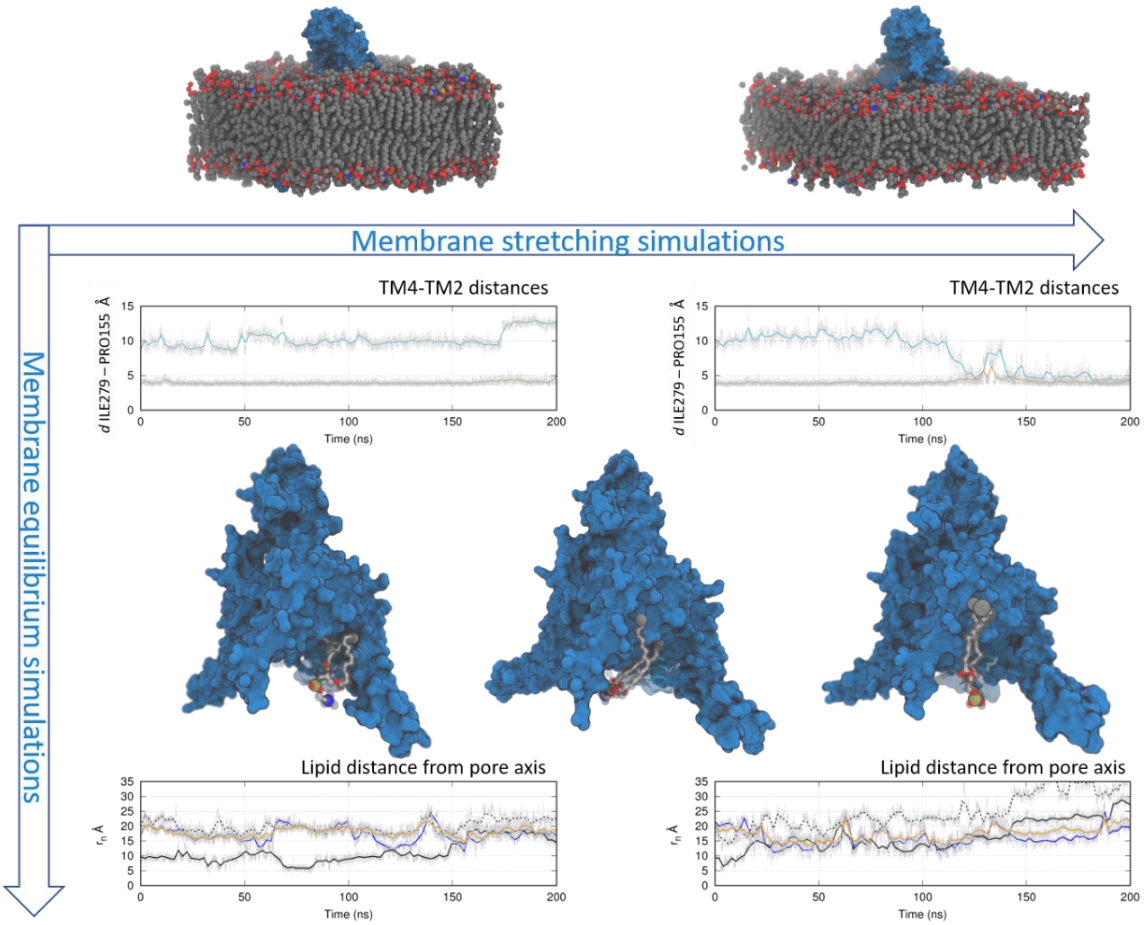

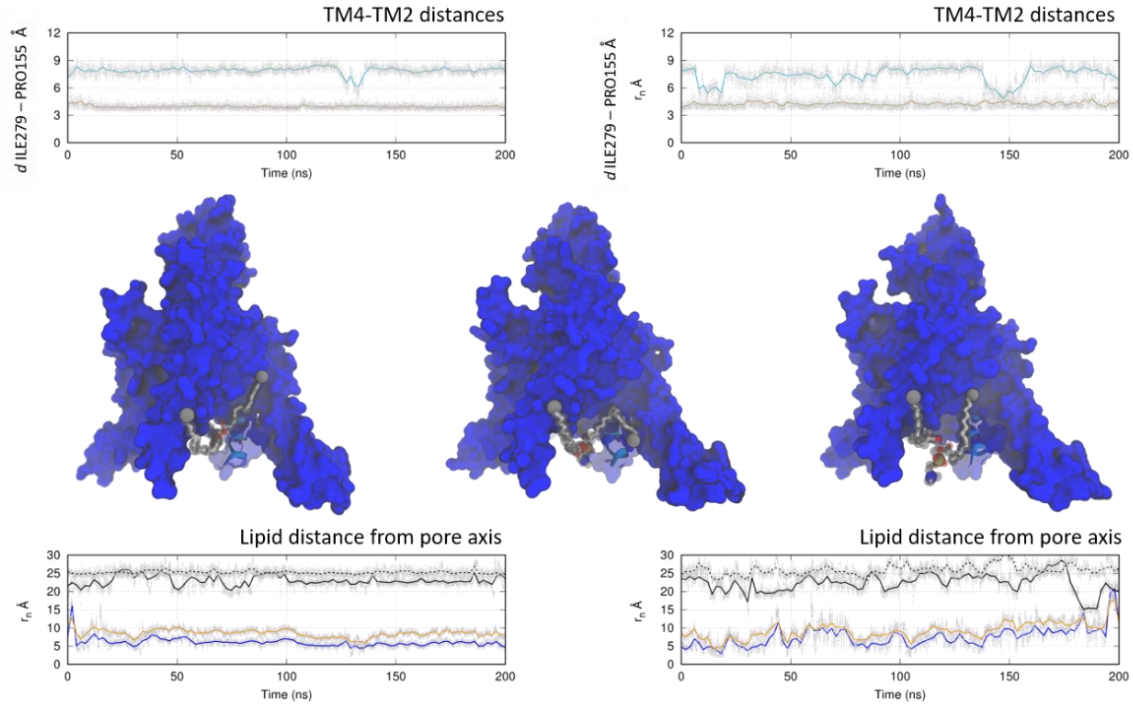

Figure 35. Schematic representation of variable parameter measured during membrane equilibrium (left panels) and membrane stretching (right panels) of considered run: -4i9w-b (top) and -4wff-c (bottom). In the upper panels are reported the distances (TM4-TM2) measured during NPT simulations and membrane stretching. The fenestration closure (TM4B-TM2A interface) is evidenced by the decreasing cyan trace during the membrane stretching simulation. In the lower panels are reported the measured distances of key atoms of the hampered lipid inside the channel cavity. The blue lines in the lower panels represent the distance of lipid N- choline moiety, the orange the P atom, bold black trace Palmitic C- terminus, the dashed black trace the Oleic C-terminus

3.3 hTRAAK in physiological conditions

3.3.1 Simulations in tandem electrostatic/concentration gradients

As a third main experiment, we wanted to test the channel ability to the conduction of potassium ions under simulative conditions mimicking physiological conditions. In this respect, we decided to start from a frame extracted from **run-4i9w-b**, in particular from the 100th ns of production phases. The system was found in symmetrical concentration of K^+ and Na^+, thus with an equally distributed concentrations of the two ions in both water bulks. Thus, the first step to mimic physiological conditions, was to apply the “energy step” method (Figure 36). After 10 ns of plain MD, the target gradient was reached, and the electrostatic potential was turned on.

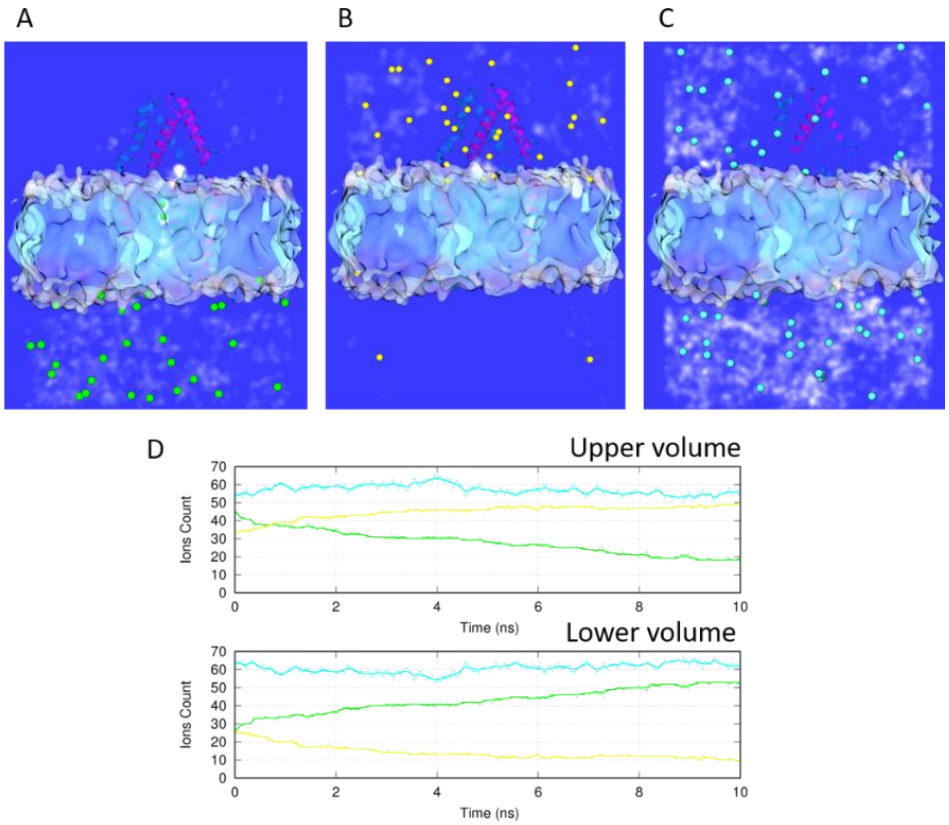

Figure 36. Volumetric maps of K^+, Na^+, Cl^- ions distributions (A, B, C respectively) in hTRAAK-POPC complex before run EF simulations. D) Ions distributions in the upper and lower volume. In Green K^+, in yellow Na^+, in cyan Cl^-.

Once the gradient was stable, simulations were started using an electrostatic potential of 100 mV (according to eq.25). All simulations were performed for 400 ns each in NVT ensemble without any restraint applied to the protein. From the electrostatic potential map, was immediately evident that the concentration gradient, did not affect the overall distribution of charges. Both water bulks, maintained approximatively the same potential, found the larger electrostatic gradient in SF proximity (Figure 37)

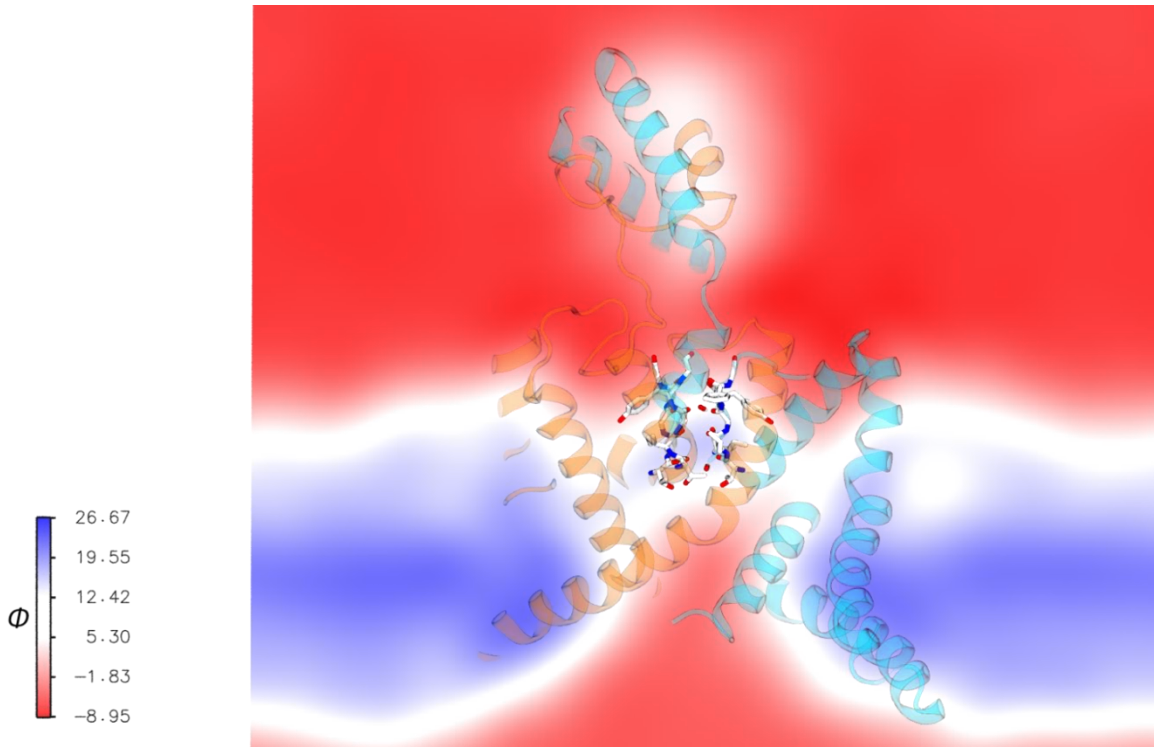

Figure 37. Electrostatic potential map of the simulation cell. The reaction potential is equally distributed over the entire cell, and the main gradient is condensed to the SF region

3.3.2 Filtration of potassium and water through the SF

The initial configuration of the Selectivity filter was set to the one previously used in other theoretical studies of K^+ permeation through potassium channel.[42,81] The selectivity was occupied by K^+ and water molecules in alternate fashion from S0 to S4 coordinating shells: [KWKWK], Figure 38. The potassium ions that were fixed in their z-Cartesian coordinates in membrane equilibrium and membrane stretching simulations, in this set of simulations were free to flow along the channel SF.

By referring to the first 500ns long simulation (**run-4i9w-EF-a**) in which ions translocations are depicted (Figure 38), after few ns of simulation, the K^+ in S0, left its coordinating slot to reach the upper water volume. The vacancy [- WKWK] was immediately replaced by the water molecule previously located in S1; the water shifted towards the upper volume, together with the other particle in a concerted translocation event. The concerted shifting, swapped the position of the vacancy within the filter at the intracellular entrance, from S0 to S4. This vacancy was promptly filled by an incoming K^+ from the intracellular side (purple

spots at ≈ 30 ns), and in few tens of ns the original configuration was restored (purple trace the S0). For the first 350 nanosecond of simulation, the translocation was constantly directed towards the upper side of the cell. Moreover, a concurrent translocation of water molecules was observed. A first complete K^+ permeation cycle was observed after 100 ns (purple trace from the intracellular to the extracellular side). For the subsequent 100 ns, the channels seemed to enter in a temporarily non-conductive state, with S0, S2, S4 occupied by K^+ and water in S1 and S3. After about 220 nanoseconds, the translocation starts again, completing four cycles of translocations. Starting from 350 ns, the channel entered an inactive state, which was maintained until the end of the simulation (500 ns).

From this first simulation, two details captured our attention: first, the translocation, when carried out, proceeded rapidly and with interposed water molecules (0-350 ns). Only after the 350 ns, the conduction stopped and the SF resulted to be dehydrated. Second, regarding the position adopted by the particles within the S3 coordinating shell, it was entirely filled by a K^+ ion only during the inactivation period, whereas it was partially filled during the conduction process, or at least in presence of a water molecule (compare time interval 100-200 ns to 350-500 ns).

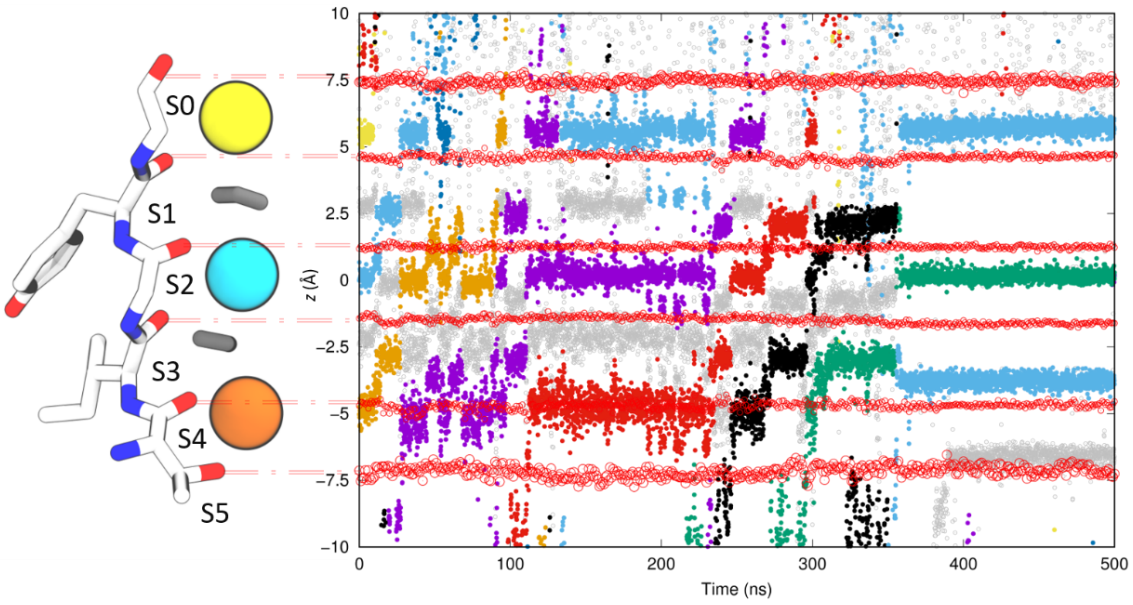

Figure 38. Conduction map through the SF. All coloured spots represent the z-Cartesian coordinates assumed by translocating ion through the channel pore. Big red dots represent the projection along the *z*-coordinates of the centre of mass calculated for each coordinating oxygens plane.

By looking at the conduction profile showed during this simulation, and more specifically to the *z*-position of the ions within the SF, we focused our attention on the single coordinating slots. Indeed, distances between opposite oxygens of each pore coordinating planes were monitored, and a surprising evidence came out: the temporal overlapping between channel inactivation and conformational alteration of the filter was exceptionally marked. After 350 ns, the distance between opposite carbonyl oxygens of THR129-THR238, and VAL239-ILE130, which equally participate to the cage-like S3 formation, were significantly reduced (Figure 39). Moreover, we note a concurrent conformational change associated to the ILE239 sidechains, changing its value from -50 to -200° during this event. Further investigations will be required to assess the relevance of this conformational transition in the inactivation of the hTRAAK filter.

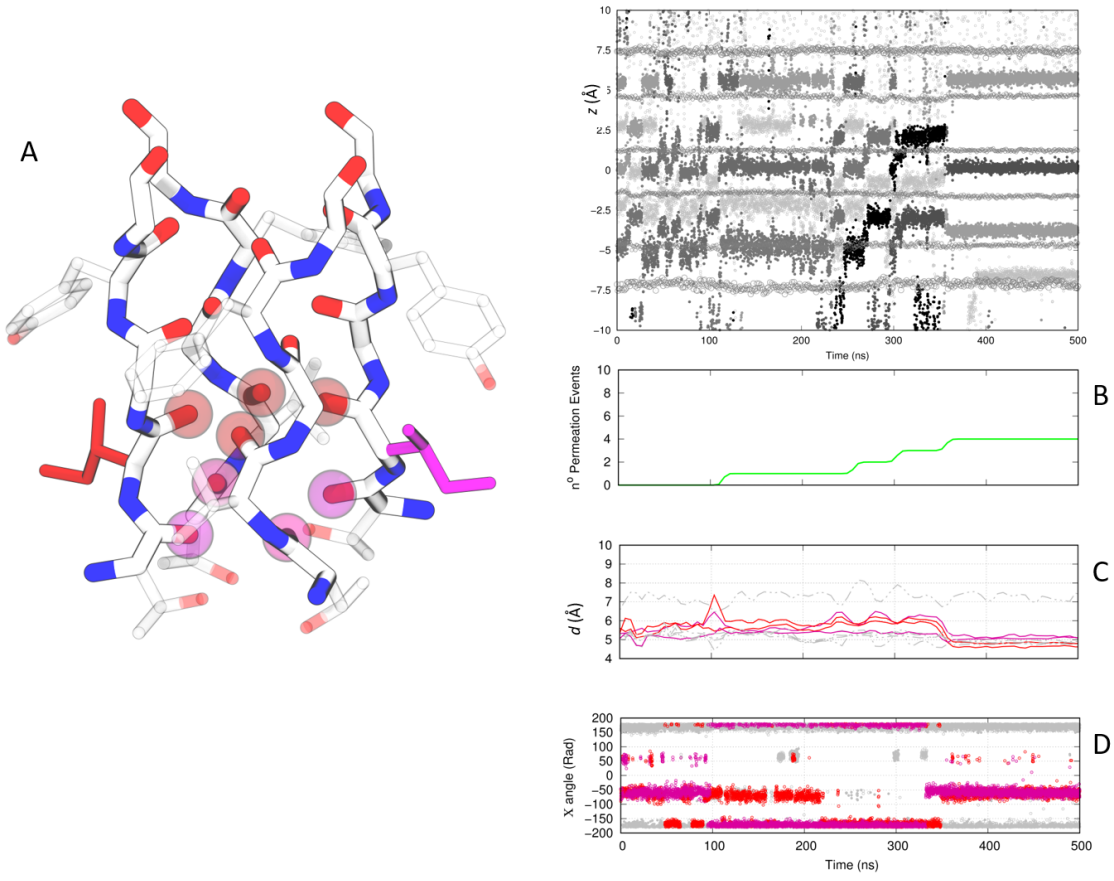

Figure 39. Conformational changings at SF level. Here reported the measurement of pnched structures adopted by the SF after the activation time (<350ns). A) SF of hTRAAK. Higlighted in red and pink (spheres) the S3 cage-like coordinating shell oxygens in pinched conformation. B) Full permeation events count, along the 500 ns run-4i9w-EF. C) Pinched related reduced distances between S3 coordinating shell oxigens. D) Time evolution of conformational changes ILE 239 sidechain χ torsional angle.

4 Conclusions & Perspectives

In this dissertation, was presented the study of a relevant and still not well characterised K2P channel protein, Human TRAAK. By using theoretical approaches belonging to computational biophysics, we provided a comprehensive characterization of the channel behaviour. Several advanced simulating conditions were used, with the purpose of mimicking as close as possible the real protein behaviour.

In this context the lipid hampering produced by protein surroundings molecules (POPC), originally proposed as putative crucial agents for the gating mechanism, was first investigated. Through the use of enhanced sampling methods (namely WTmetaD simulations), we investigated the influence of the lipid to the flow of cations towards the SF. It was found that individual lipids can indeed interact with the intercellular SF domain, potentially hindering the K^+ translocations.

After these encouraging results, we chose to investigate the role of the bilayer on the modulation of the channel. In this context, repeated runs were performed starting from distinct crystal structures, to observe and characterize conformational transitions promoted by the membrane stretching. A putative channel gating mechanism involving theTM4s inner helices was therefore elucidated.

Finally, using a third strategy, asymmetric ionic concentrations were generated across the simulation cell, and electrostatic potential was applied in order to mimic physiological conditions. This setup allowed us to characterize the K^+ translocation process through the Selectivity Filter, and a putative C-type inactivation mechanism was identified. Indeed, a pinched SF conformation was observed which is most likely involved in the channel inactivation process.

The simulations performed in this thesis provide useful insights on the modulation mechanism of the hTRAAK channel. However, future work is required to fully characterize these aspects either from a qualitative and quantitative standpoint.

5 Bibliography

1. Eisenberg, R. S. *Channels as Enzymes*. *J. Membrane Biol* **115,** (1990).

2. Lansman, J. B., Hallam, T. J. & Rink, T. J. Single stretch-activated ion channels in vascular endothelial cells as mechanotransducers? *Nature* **325,** 811–813 (1987).

3. Ashcroft, F. M. & Rorsman, P. KATP channels and islet hormone secretion: new insights and controversies. *Nat. Rev. Endocrinol.* **9,** 660–669 (2013).

4. McDonald, T. F., Pelzer, S., Trautwein, W. & Pelzer, D. J. Regulation and modulation of calcium channels in cardiac, skeletal, and smooth muscle cells. *Physiol. Rev.* **74,** 365–507 (1994).

5. Jiang, Y. *et al.* The open pore conformation of potassium channels. *Nature* **417,** 523–526 (2002).

6. Choe, S. Potassium channel structures. *Nat. Rev. Neurosci.* **3,** 115–121 (2002).

7. Catterall, W. A. Structure and Function of Voltage-Gated Ion Channels. *Annu. Rev. Biochem.* **64,** 493–531 (1995).

8. Collingridge, G. L. & Olsen, R. W. A nomenclature for ligand-gated ion channels. *Neuropharmacology* **56,** 2–5 (2009).

9. Nichols, C. G. & Lopatin, A. N. INWARD RECTIFIER POTASSIUM CHANNELS. *Annu. Rev. Physiol.* **59,** 171–191 (1997).

10. Goldstein, S. A. N., Bockenhauer, D., O'Kelly, I. & Zilberberg, N. Potassium leak channels and the KCNK family of two-p-domain subunits. *Nat. Rev. Neurosci.* **2,** 175–184 (2001).

11. Smyth, M. S. & Martin, J. H. x ray crystallography. *Mol. Pathol.* **53,** 8–14 (2000).

12. Doyle, D. A. The Structure of the Potassium Channel: Molecular Basis of K+ Conduction and Selectivity. *Science (80-.).* **280,** 69–77 (1998).

13. Ketchum, K. A., Joiner, W. J., Sellers, A. J., Kaczmarek, L. K. & Goldstein, S. A. N. A new family of outwardly rectifying potassium channel proteins with two pore domains in tandem. *Nature* **376,** 690–695 (1995).

14. HODGKIN, A. L. & HUXLEY, A. F. A quantitative description of membrane current and its application to conduction and excitation in nerve. *J. Physiol.* **117,** 500–44 (1952).

15. Lesage, F. *et al.* TWIK-1, a ubiquitous human weakly inward

rectifying K+ channel with a novel structure. *EMBO J.* **15,** 1004–11 (1996).

16. Lotshaw, D. P. Biophysical, pharmacological, and functional characteristics of cloned and native mammalian two-pore domain K+ channels. *Cell Biochem. Biophys.* **47,** 209–256 (2007).

17. Brohawn, S. G., del Marmol, J. & MacKinnon, R. Crystal Structure of the Human K2P TRAAK, a Lipid- and Mechano-Sensitive K+ Ion Channel. *Science (80-.).* **335,** 436–441 (2012).

18. Enyedi, P. & Czirjak, G. Molecular Background of Leak K+ Currents: Two-Pore Domain Potassium Channels. *Physiol. Rev.* **90,** 559–605 (2010).

19. Cadaveira-Mosquera, A. *et al.* Expression of K2P Channels in Sensory and Motor Neurons of the Autonomic Nervous System. *J. Mol. Neurosci.* **48,** 86–96 (2012).

20. Hughes, S., Foster, R. G., Peirson, S. N. & Hankins, M. W. Expression and localisation of two-pore domain (K2P) background leak potassium ion channels in the mouse retina. *Sci. Rep.* **7,** 46085 (2017).

21. Brohawn, S. G., Campbell, E. B. & MacKinnon, R. Physical mechanism for gating and mechanosensitivity of the human TRAAK K+ channel. *Nature* **516,** 126–130 (2014).

22. Mi Hwang, E. *et al.* A disulphide-linked heterodimer of TWIK-1 and TREK-1 mediates passive conductance in astrocytes. *Nat. Commun.* **5,** 3227 (2014).

23. Bockenhauer, D., Zilberberg, N. & Goldstein, S. A. N. KCNK2: reversible conversion of a hippocampal potassium leak into a voltage-dependent channel. *Nat. Neurosci.* **4,** 486–491 (2001).

24. Maingret, F., Patel, A. J., Lesage, F., Lazdunski, M. & Honoré, E. Lysophospholipids open the two-pore domain mechano-gated K(+) channels TREK-1 and TRAAK. *J. Biol. Chem.* **275,** 10128–33 (2000).

25. Patel, A. J. *et al.* Inhalational anesthetics activate two-pore-domain background K+ channels. *Nat. Neurosci.* **2,** 422–426 (1999).

26. Franks, N. P. & Honoré, E. The TREK K2P channels and their role in general anaesthesia and neuroprotection. *Trends Pharmacol. Sci.* **25,** 601–608 (2004).

27. Heurteaux, C. *et al.* TREK-1, a K+ channel involved in neuroprotection and general anesthesia. *EMBO J.* **23,** 2684–95 (2004).

28. Noël, J. *et al.* The mechano-activated K+ channels TRAAK and TREK-1 control both warm and cold perception. *EMBO J.* **28,**

1308–1318 (2009).

29. Bagriantsev, S. N. *et al.* Multiple modalities converge on a common gate to control K2P channel function. *EMBO J.* **30,** 3594–606 (2011).

30. Bayliss, D. A. & Barrett, P. Q. Emerging roles for two-pore-domain potassium channels and their potential therapeutic impact. *Trends Pharmacol. Sci.* **29,** 566–575 (2008).

31. Kim, Y., Gnatenco, C., Bang, H. & Kim, D. Localization of TREK-2 K + channel domains that regulate channel kinetics and sensitivity to pressure, fatty acids and pH i. *Pfl**gers Arch. Eur. J. Physiol.* **442,** 952–960 (2001).

32. Dror, R. O., Dirks, R. M., Grossman, J. P., Xu, H. & Shaw, D. E. Biomolecular Simulation: A Computational Microscope for Molecular Biology. (2012). doi:10.1146/annurev-biophys-042910-155245

33. Hamill, O. P. & Martinac, B. Molecular Basis of Mechanotransduction in Living Cells. *Physiol. Rev.* **81,** 685–740 (2001).

34. Brohawn, S. G. How ion channels sense mechanical force: insights from mechanosensitive K2P channels TRAAK, TREK1,

and TREK2. *Ann. N. Y. Acad. Sci.* **1352,** 20–32 (2015).

35. XIANTAOLI, X. T. *et al.* The stretch-activated potassium channel TREK-1 in rat cardiac ventricular muscle. *Cardiovasc. Res.* **69,** 86–97 (2006).

36. Maingret, F., Fosset, M., Lesage, F., Lazdunski, M. & Honoré, E. TRAAK is a mammalian neuronal mechano-gated K+ channel. *J. Biol. Chem.* **274,** 1381–7 (1999).

37. Brohawn, S. G., Su, Z. & Mackinnon, R. Mechanosensitivity is mediated directly by the lipid membrane in TRAAK and TREK1 K + channels. doi:10.1073/pnas.1320768111

38. Zhou, Y., Morais-Cabral, J. H., Kaufman, A. & MacKinnon, R. Chemistry of ion coordination and hydration revealed by a K+ channel–Fab complex at 2.0Å resolution. *Nature* **414,** 43–48 (2001).

39. Bucher, D., Guidoni, L., Carloni, P. & Rothlisberger, U. Coordination Numbers of K+ and Na+ Ions Inside the Selectivity Filter of the KcsA Potassium Channel: Insights from First Principles Molecular Dynamics. *Biophys. J.* **98,** L47–L49 (2010).

40. Cordero-Morales, J. F. *et al.* Molecular determinants of gating at the potassium-channel selectivity filter. *Nat. Struct. Mol. Biol.* **13,** (2006).

41. Domene, C., Klein, M. L., Branduardi, D., Gervasio, F. L. & Parrinello, M. Conformational Changes and Gating at the Selectivity Filter of Potassium Channels. *J. Am. Chem. Soc.* **130,** 9474–9480 (2008).

42. Oakes, V., Furini, S., Pryde, D. & Domene, C. Exploring the Dynamics of the TWIK-1 Channel. *Biophys. J.* **111,** 775–784 (2016).

43. Aryal, P., Abd-Wahab, F., Bucci, G., Sansom, M. S. & Tucker, S. J. Influence of lipids on the hydrophobic barrier within the pore of the TWIK-1 K2P channel. *Channels* **9,** 44–49 (2015).

44. Brohawn, S. G., Campbell, E. B. & Mackinnon, R. Domain-swapped chain connectivity and gated membrane access in a Fab-mediated crystal of the human TRAAK K + channel. doi:10.1073/pnas.1218950110

45. Jacobson, M. P. *et al.* A hierarchical approach to all-atom protein loop prediction. *Proteins Struct. Funct. Bioinforma.* **55,** 351–367 (2004).

46. Madhavi Sastry, G., Adzhigirey, M., Day, T., Annabhimoju, R. & Sherman, W. Protein and ligand preparation: parameters, protocols, and influence on virtual screening enrichments. doi:10.1007/s10822-013-9644-8

47. Humphrey, W., Dalke, A. & Schulten, K. VMD: Visual molecular dynamics. *J. Mol. Graph.* **14,** 33–38 (1996).

48. Decherchi, S., Bottegoni, G., Spitaleri, A., Rocchia, W. & Cavalli, A. BiKi Life Sciences: A New Suite for Molecular Dynamics and Related Methods in Drug Discovery. *J. Chem. Inf. Model.* **58,** 219–224 (2018).

49. Phillips, J. C. *et al.* Scalable molecular dynamics with NAMD. *J. Comput. Chem.* **26,** 1781–1802 (2005).

50. Klauda, J. B. *et al.* Update of the CHARMM all-atom additive force field for lipids: validation on six lipid types. *J. Phys. Chem. B* **114,** 7830–43 (2010).

51. Feller, S. E., Zhang, Y., Pastor, R. W. & Brooks, B. R. Constant pressure molecular dynamics simulation: The Langevin piston method. *J. Chem. Phys.* **103,** 4613–4621 (1995).

52. Ryckaert, J.-P., Ciccotti+, G. & Berendsen, H. J. C. *Numerical integration of the Cartesian Equations of Motion of a System with Constraints: Molecular Dynamics of n-Alkanes*. *JOURNAL OF COMPUTATIONAL. PHYSICS* **23,** (1977).

53. Essmann, U. *et al.* A smooth particle mesh Ewald method. *J. Chem. Phys.* **103,** 8577–8593 (1995).

54. Bonomi, M. *et al.* PLUMED: a portable plugin for free-energy calculations with molecular dynamics. (2009). doi:10.1016/j.cpc.2009.05.011

55. Barducci, A., Bussi, G. & Parrinello, M. Well-Tempered Metadynamics: A Smoothly Converging and Tunable Free-Energy Method. *Phys. Rev. Lett.* **100,** 020603 (2008).

56. Laio, A. & Parrinello, M. Escaping free-energy minima. *Proc. Natl. Acad. Sci. U. S. A.* **99,** 12562–6 (2002).

57. Barducci, A., Bonomi, M. & Parrinello, M. Advanced Review Metadynamics. *Ltd. WIREs Comput Mol Sci* **1,** 826–843 (2011).

58. Berendsen, H. J. C., van der Spoel, D. & van Drunen, R. GROMACS: A message-passing parallel molecular dynamics implementation. *Comput. Phys. Commun.* **91,** 43–56 (1995).

59. Bussi, G., Donadio, D. & Parrinello, M. *Canonical sampling through velocity-rescaling*. (2008).

60. Parrinello, M. & Rahman, A. Polymorphic transitions in single crystals: A new molecular dynamics method. *J. Appl. Phys.* **52,** 7182–7190 (1981).

61. Nosé, S. A unified formulation of the constant temperature molecular dynamics methods. *J. Chem. Phys.* **81,** 511–519

(1984).

62. Hoover, W. G. Canonical dynamics: Equilibrium phase-space distributions. *Phys. Rev. A* **31,** 1695–1697 (1985).

63. Hess, B., Bekker, H., Berendsen, H. J. C. & Fraaije, J. G. E. M. LINCS: A linear constraint solver for molecular simulations. *J. Comput. Chem.* **18,** 1463–1472 (1997).

64. Kučerka, N., Tristram-Nagle, S. & Nagle, J. F. Structure of Fully Hydrated Fluid Phase Lipid Bilayers with Monounsaturated Chains. *J. Membr. Biol.* **208,** 193–202 (2006).

65. Seelig, J. & Waespe-Sarcevic, N. Molecular order in cis and trans unsaturated phospholipid bilayers. *Biochemistry* **17,** 3310–3315 (1978).

66. Allen, W. J., Lemkul, J. A. & Bevan, D. R. GridMAT-MD: A grid-based membrane analysis tool for use with molecular dynamics. *J. Comput. Chem.* **30,** 1952–1958 (2009).

67. Leontiadou, H., Mark, A. E. & Marrink, S. J. Molecular Dynamics Simulations of Hydrophilic Pores in Lipid Bilayers. *Biophys. J.* **86,** 2156–2164 (2004).

68. Xie, J. Y., Ding, G. H. & Karttunen, M. Molecular dynamics simulations of lipid membranes with lateral force: Rupture and

dynamic properties. *Biochim. Biophys. Acta - Biomembr.* **1838,** 994–1002 (2014).

69. Gullingsrud, J. & Schulten, K. Lipid Bilayer Pressure Profiles and Mechanosensitive Channel Gating. *Biophys. J.* **86,** 3496–3509 (2004).

70. Berger, O., Edholm, O. & Jähnig, F. Molecular dynamics simulations of a fluid bilayer of dipalmitoylphosphatidylcholine at full hydration, constant pressure, and constant temperature. *Biophys. J.* **72,** 2002–2013 (1997).

71. Sotomayor, M. & Schulten, K. Molecular Dynamics Study of Gating in the Mechanosensitive Channel of Small Conductance MscS. *Biophys. J.* **87,** 3050–3065 (2004).

72. Aryal, P. *et al.* Bilayer-Mediated Structural Transitions Control Mechanosensitivity of the TREK-2 K2P Channel. *Structure* **25,** 708–718.e2 (2017).

73. Kalra, A., Garde, S. & Hummer, G. Osmotic water transport through carbon nanotube membranes. *Proc. Natl. Acad. Sci. U. S. A.* **100,** 10175–80 (2003).

74. Kutzner, C., Grubmüller, H., de Groot, B. L. & Zachariae, U. Computational electrophysiology: the molecular dynamics of ion channel permeation and selectivity in atomistic detail.

Biophys. J. **101,** 809–17 (2011).

75. Khalili-Araghi, F., Ziervogel, B., Gumbart, J. C. & Roux, B. Molecular dynamics simulations of membrane proteins under asymmetric ionic concentrations. *J. Gen. Physiol.* **142,** 465–475 (2013).

76. Treptow, W., Maigret, B., Chipot, C. & Tarek, M. Coupled Motions between Pore and Voltage-Sensor Domains: A Model for Shaker B, a Voltage-Gated Potassium Channel. doi:10.1529/biophysj.104.039628

77. Jensen, M. O. *et al.* Principles of conduction and hydrophobic gating in K+ channels. *Proc. Natl. Acad. Sci.* **107,** 5833–5838 (2010).

78. Gumbart, J., Khalili-Araghi, F., Sotomayor, M. & Roux, B. Constant electric field simulations of the membrane potential illustrated with simple systems. *Biochim. Biophys. Acta - Biomembr.* **1818,** 294–302 (2012).

79. Aksimentiev, A. & Sotomayor, M. *Electrostatic Maps and Ion Conduction*. (2006).

80. Berneche, S. & Roux, B. A microscopic view of ion conduction through the K+ channel. *Proc. Natl. Acad. Sci.* **100,** 8644–8648 (2003).

81. Ceccarini, L., Masetti, M., Cavalli, A. & Recanatini, M. Ion Conduction through the hERG Potassium Channel. *PLoS One* **7,** e49017 (2012).